Faculty of Engineering

Investigation on Mixing Performance and Droplet Generation of Dissimilar Liquids through T-junction and Offset T-junction Microchannels

Hawa Anak Ringkai

Master of Engineering
2022

Investigation on Mixing Performance and Droplet Generation of Dissimilar Liquids through T-junction and Offset T-junction Microchannels

Hawa Anak Ringkai

A thesis submitted

In fulfillment of the requirements for the degree of Master of Engineering

(Mechanical Engineering)

Faculty of Engineering
UNIVERSITI MALAYSIA SARAWAK
2022

DECLARATION

I declare that the work in this thesis was carried out in accordance with the regulations of Universiti Malaysia Sarawak. Except where due acknowledgements have been made, the work is that of the author alone. The thesis has not been accepted for any degree and is not concurrently submitted in candidature of any other degree.

……

Signature

Name: Hawa Anak Ringkai

Matric No.: 19020160

Faculty of Engineering

Universiti Malaysia Sarawak

Date: 02 July 2022

ACKNOWLEDGEMENT

I would like to express my deepest appreciation to Ir. Dr. Khairul Fikri bin Tamrin, my supervisor for the assistance and helpful guidance throughout this project. I am also grateful for the professionalism, compassion and patience shown by him during this period that helped me a lot toward the completion of this project.

My sincere gratitude to the lecturers and friends, especially from the Department of Mechanical and Manufacturing Engineering, Faculty of Engineering UNIMAS, for the continuous advice and support given throughout this project period. This research is fully-supported by the UNIMAS Zamalah Graduate Scholarship (ZSU).

Finally, yet importantly, I would like to pay my highest respect to my family, who keeps giving me positive motivation towards life and challenges, to strengthen me, both physically and mentally.

Thank you.

ABSTRACT

To date, microfluidic device has contributed significantly in biotechnology and life sciences due to their fast response time, low consumption of samples and high sensitivity. Although it is widely utilized in bio-, nano-, and environmental technologies, there are still limited experimental investigations on the micromixing process of dissimilar liquids i.e., in cosmetics, construction and biofuel production. In this study, the mixing index of propan-2-ol and water, water and sodium chloride solution, propan-2-ol and sodium chloride solution were characterized and reported at $5 \leq Re \leq 50$ inside the 750 µm-radius of fabricated T-junction and offset T-junction microfluidic channel. By using RGB colour model method, both microchannels for miscible mixing experiments show better mixing index at high Reynolds number (Re) of 40 and 50 due to the significant convection which is caused by the effect of stretching and thinning of liquid lamellae. Meanwhile, for immiscible mixture, offset T-junction yielded superior mixing performance than T-junction microchannel at both low and high Re. Hence, due to the fact that offset T-junction performs better than T-junction, the study was furthered by investigating the behaviours of water-in-oil droplet at interfacial surface within offset T-junction microchannel having different size i.e., radius of 400 µm, 500 µm, 750 µm and 1000 µm using micro-PIV software. The results showed that experimental velocity of the water droplet holds good agreement with theoretical values, having minimal difference as low as 0.004 mm/s for the case of microchannel with radius 750 µm. A maintained average velocity of 0.055 mm/s for channel with radius of 1000 µm was achieved, meanwhile the other channels showed a good average velocity data i.e., an increase from 0.15 mm/s to 0.20 mm/s for channel radius of 500 µm. In addition, a major elevation for mean velocity from 0.055 mm/s to 0.15 mm/s for channel with radius of 750 µm was also seen. The proposed design of microfluidic

device especially offset T-junction offers more efficient and better results in micromixing study of immiscible liquids.

Keywords: Microfluidic, micromixing, T-junction, droplet, micro-PIV

Pencirian Prestasi Pencampuran dan Penghasilan Titisan dalam Fabrikasi Peranti Mikrofluidik Simpang-T dan Pengimbang Simpang-T

ABSTRAK

Sehingga kini, alat mikrofluidik telah memberikan sumbangan yang besar dalam bioteknologi dan sains kehidupan kerana masa tindak balasnya yang cepat, penggunaan sampel yang rendah dan kepekaan yang tinggi. Walaupun digunakan secara meluas dalam teknologi bio, nano, dan alam sekitar , masih ada kajian eksperimental yang terhad mengenai proses pencampuran mikro cecair yang tidak serupa, iaitu dalam kosmetik, pembinaan dan pengeluaran biofuel. Dalam kajian ini, indeks pencampuran propan-2-ol dan air, air dan larutan natrium klorida, propan-2-ol dan larutan natrium klorida dicirikan dan dilaporkan pada $5 \leq Re \leq 50$ *di dalam 750 µm-radius saluran mikrofluidik simpang-T dan pengimbang simpang-T. Dengan menggunakan kaedah model warna RGB, kedua-dua saluran mikro untuk eksperimen pencampuran cecair boleh larut menunjukkan indeks pencampuran yang lebih baik pada bilangan Reynolds yang tinggi iaitu 40 dan 50 kerana perolakan yang ketara yang disebabkan oleh kesan regangan dan penipisan lamela cecair. Sementara itu, untuk pencampuran cecair tidak larut, pengimbang simpang-T menghasilkan prestasi pencampuran yang lebih baik daripada saluran mikro simpang-T pada bilangan Reynolds rendah dan tinggi. Oleh itu, disebabkan oleh fakta bahawa pengimbang simpang-T menunjukkan prestasi lebih baik daripada simppang-T, kajian ini dilanjutkan dengan menyiasat kelakuan titisan air dalam minyak pada permukaan antara muka dalam saluran mikro pengimbang simpang-T dengan saiz yang berbeza iaitu, jejari 400 µm, 500 µm, 750 µm dan 1000 µm menggunakan perisian mikro-PIV. Hasil kajian menunjukkan bahawa halaju eksperimen titisan air dalam persamaan dengan nilai teori, dengan perbezaan minimum serendah 0.004 mm/s untuk kes saluran mikro dengan jejari*

750 µm. Pengekalan halaju purata sebanyak 0.055 mm/s untuk saluran jejari 1000 µm dicapai, sementara saluran lain menunjukkan data halaju rata-rata yang baik, iaitu peningkatan dari 0.15 mm/s ke 0.20 mm/s untuk saluran jejari 500 µm. Selain itu, peningkatan terbanyak untuk halaju min dari 0.055 mm/s ke 0.15 mm/s untuk saluran jejari 750 µm juga terlihat. Reka bentuk yang dicadangkan bagi alat mikrofluidik terutamanya pengimbang simpang-T menawarkan hasil yang lebih cekap dan lebih baik dalam kajian pencampuran mikro cecair tidak larut.

Kata kunci: *Mikrofluidik, pencampuran mikro, simpang-T, titisan, mikro-PIV*

TABLE OF CONTENTS

LIST OF TABLES

LIST OF FIGURES

Page

LIST OF ABBREVIATIONS

CCD	Charge-coupled device
CFD	Computational Fluid Dynamics
DC	Direct current
IOS	Intensity of Segregation
MATLAB	Matrix laboratory
MEMS	Microelectromechanical system
Nd: YLF	Neodymium-doped yttrium lithium fluoride
NEMA	National Electrical Manufacturers Association
NIH	National Institutes of Health
p-ATP	Paminothiophenol
PDMS	Polydimethylsiloxane
PIV	Particle image velocimetry
PLIF	Planar laser induced fluorescence
PMMA	Poly (methyl methacrylate)
Re	Reynolds number
RGB	Red, green, blue
SERS	Surface enhanced Raman scattering
μ-LIF	Micro-laser induced fluorescence
μTAS	Micrototal analysis system

CHAPTER 1

INTRODUCTION

1.1 Chapter Overview

This chapter provides a brief introduction of microfluidic device's applications and its purposes, particularly focuses on the micromixing and droplet generation. The past studies on these applications, mainly on their methods will be described in Section 1.2. Besides that, Section 1.3 clearly describes the problem statements that discuss the existing issue and problems in micromixing and droplet generation studies, respectively. Section 1.4 elaborated the overall scope of this study, meanwhile the hypothesis can be found in Section 1.5. Furthermore, the research objectives of the overall experimental study will be stated in Section 1.6. Finally, the structure and summary of this thesis will be provided at the end of this chapter, which is in Section 1.7.

1.2 Background Study

Over the years, microfluidic devices have been developed significantly for microelectromechanical system (MEMS), microchemical technology and micrototal analysis system (μTAS). For instance, micromixing process in microfluidic devices has been widely employed in bio-, nano-, and environmental technologies for biomedical and health related issues (Kim & Yoon, 2017; Kumar Mondal & Wongwises, 2020). It also extensively applied in food and chemical industries. Generally, most of the applications either involve use of miscible or immiscible liquids (Fornerod et al., 2020). A miscible liquid is a liquid that mixes homogeneously with one another, whereas the immiscible does not dissolve in any liquids and will form two distinctive layers.

The purposes of mixing in microfluidic device are to improve the efficiency of mixing by reducing the characteristics size of microscale devices within shorter mixing channels (Lee et al., 2011), and reduce the cost of laboratory equipment as it diminishes the consumption of specimens (Solehati et al., 2014; Viktorov et al., 2016). In addition, fast and complete mixing of different samples of fluids also can be achieved in this microfluidic devices/geometry. In general, the mixing of the liquid sample species in microfluidic devices under different configurations is majorly dominated by diffusion process (Lee et al., 2011). However, microscale mixing remains a challenge due to the inefficient mixing in microfluidics system (Shah et al., 2019b) which is primarily governed by slow molecular diffusion (Lee & Fu, 2018) since the mixing time is directly proportional to the square of the channel width over the molecular diffusivity (Aubin et al., 2010).

To better understand the micromixing process, there are a number of numerical studies on the micromixing of different densities and viscosities liquids i.e., water-ethanol mixtures (Jeon et al., 2004; Lin et al., 2007; Wang et al., 2002). Ansari et al. (2010) numerically investigated the mixing performance influenced by the water and ethanol stream interface's positions inside T-junction microchannels at $0 < Re \leq 10$. It was found that the interface's position in the channel for low $Re < 10$ had a major impact on mixing efficiency. Chung and Shih (2008) used a planar micromixer with rhombic microchannels and a converging-diverging element to study the mixing of ethanol and water, and found that over 90% mixing can be achieved at 30° turning angle and $Re \geq 200$. This proved that the rhombic micromixer has potential to be used in the future applications of fast and high throughput mixing. Orsi et al. (2013) performed numerical study on the mixing behaviours of water-ethanol in T-junction microchannel for Re ranging from 1 to 300 via a commercial Computational Fluid Dynamics (CFD) software. The numerical data showed a good mixing

performance of water-ethanol at Re < 100 due to high viscosity of ethanol and therefore lead to high residence time of the liquids occupying the interfacial region. Meanwhile, at high Re, water and ethanol streams were separated by a viscous layer led to vortex formation and poor mixing.

Apart from micromixing, the multiphase flow, especially two-phase flow, also occurs so often in the aforementioned microfluidic device applications (Fu et al., 2009). For example, liquid-liquid multiphase flow has numerous applications in mixing process (Günther et al., 2005; J. Wang et al., 2015), chemical reaction (Wu et al., 2019), and also the emulsion technology (Chen et al., 2009; Vladisavljević et al., 2017). One important application of these devices is the generation of monodisperse emulsions and particles that have precise size and composition (Joensson & Andersson, 2012; Li et al., 2017; Teh et al., 2008). The device rely on the co-axial flow of these immiscible liquids and breaking-up the disperse phase into droplets suspended in the outer continuous liquid with the resulting shear forces through geometric constriction (Shah et al., 2008).

The common geometries used for the microfluidic droplet generation are flow-focusing, co-flow and cross-flow devices. For example, Thurgood et al. (2019) used polydimethylsiloxane (PDMS) based microfluidic flow-focusing channel to investigate the size, gap and generation rate of oil-in-water droplets (refer to Figure 1.1). The ability of asynchronous oil droplet generation with the gap varying from few microns to few hundred microns in successive and rapid cycles was highlighted in the study. Deng et al. (2018) studied the hydrodynamics of rising droplets i.e., soybean oil and toluene in quiescent water using co-flowing microfluidic device. The results of the experimentations indicated the rigid-sphere like behaviour of single micro-droplet in terms of its terminal velocity; however, the swarm of droplets moves with a higher terminal velocity as compared to a

single droplet. Yao et al. (2019) investigated the effect of different viscosities of carrier oil on water-in-oil emulsion using a cross-flow T-junction microchannel. The results showed that regard-less of the flow pressure levels, the droplet size and droplet generation rate decreased as the oil viscosity increased. Based on these three types of microfluidic droplet generation geometries, cross-flow is the simplest and most used geometry to generate droplets in a controlled way (Zhu & Wang, 2017).

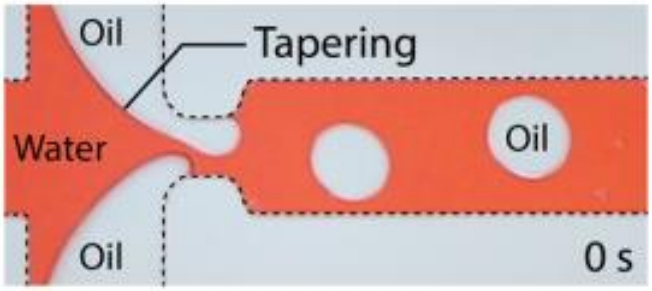

Figure 1.1: Generation of oil droplets in water within the flow-focusing channel (Thurgood et al., 2019)

Literally, producing oil-in-water droplets is easier than developing their water-in-oil droplets (Colucci et al., 2020). Suspended water droplets is significant such as encapsulating the bioactive compounds for controlled release in fat-based edible products (Zhu et al., 2019). As in droplet based microfluidics experiment, Yao et al. (2019) investigated the effect of different viscosities of carrier oil on water-in-oil emulsion using a cross-flow device which is T-junction microchannel (refer to Figure 1.2). The results indicated that with the increase of oil viscosity, the size of droplet decreased and this happened regardless of pressure level of flow.

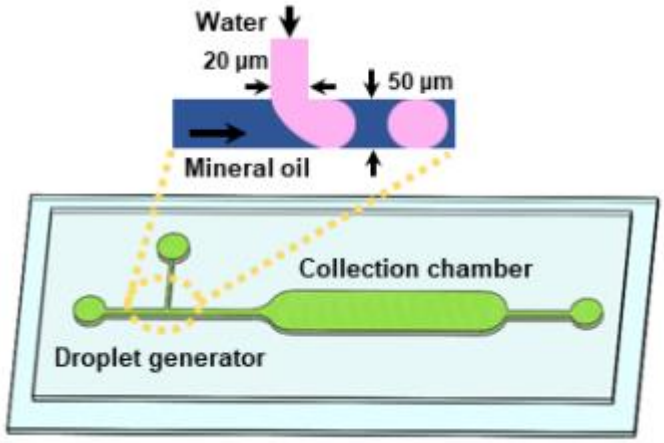

Figure 1.2: Water-in-oil emulsion using cross-flow microchannel (Yao et al., 2019)

Micro particle image velocimetry (micro-PIV) method has been widely known technique in the application of microfluidics (Campo-Deaño, 2018; Hagsäter et al., 2007; Omori et al., 2015; Santiago et al., 1998; Shinohara et al., 2004). Moreover, the internal flow details of the droplet in the microchannels have been characterized mostly by this technique due to its capability to obtain instantaneous velocity measurements and related properties in fluids (Hein et al., 2015; Jakiela et al., 2012; Liu et al., 2017; Ma et al., 2014, 2015; Oishi et al., 2011). There are a number of studies involving the use of this method to study the formation of droplets. Liu et al. (2017) investigated the internal flow field of water-in-oil droplets flowing in a T-junction microchannel using micro-PIV method. One important observation is the impact of the capillary number on the flow physics including its critical value, while geometry of the droplet impacts the axial as well as transverse velocity components. Kinoshita et al. (2007) computed and visualized the internal flow of a flowing water/glycerol-in-oil droplet in PDMS T-junction microchannel using confocal micro-PIV system. The measured results revealed that the fluid residing inside the droplet intricately observes a circular three-dimensional motion within the constrained volume as

the contacting surfaces, i.e., surrounding walls of the channel, pose drag on the surfaces of the droplet while it moves inside the microchannel. This complex fluid motion within a droplet improves mixing and resultantly chemical reaction in the device, if any.

1.3 Problem Statement

The mixing process involving dissimilar miscible liquids holds great importance in numerous industrial applications (Table 1.1). However, in respect to microfluidics, there are limited experimental investigations that look into the mixing process between two distinct miscible liquids. For example, Lin et al. (2007) experimentally investigated the mixing of ethanol and water using T-junction microchannel having J-shaped baffle. Due to unequal lateral perturbation, it was found that the mixing performance increases with the increase of baffle number as high convection and molecular redistribution occurred along the main channel. Wang et al. (2012) investigated micromixing of water-water and water-ethanol in T-junction microchannel. Mixing performance of water-ethanol was found better than that of water-water due to the former having dissimilar densities which effectively improved driving force of mass transfer at the interface. To the best of authors' knowledge, there are also limited studies on experimental investigation and characterization of mixing performance of two immiscible liquids.

Table 1.1: Mixing process of dissimilar miscible liquids in industry

Liquid A	Liquid B	Industrial applications
Propan-2-ol	Water	Solvents for cosmetics, antiseptic and cleaning solutions in chemical and pharmaceutical industries.
Water	Sodium chloride solution	Creates saline solution, which can be useful in medical treatment (Nagata, 2018) i.e., cleaning wounds, and also in construction i.e., mixing

		and curing on the strength of concrete (Giasuddin et al., 2013).
Propan-2-ol	Sodium chloride solution	The mixture salting out process is useful for production of clean and renewable biofuels (Li et al., 2019), results in the separation of the alcohol from the mixture and formation of a two-phase system (Heydari & Mousavi, 2016; Xie et al., 2016).

Meanwhile, in a different study i.e., droplet generation process, Jin and Yoo (2012) conducted flow visualization via micro-PIV to investigate water/glycerol-in-oil droplet merging processes in a main Y-microchannel which is connected downstream to a straight channel or a divergent channel. The results for a straight channel confined droplet suggest that the rear droplets, at the time coalescence, penetrated the front droplets. While in the divergent channel geometry, as the droplet merges a strong vortex motion is generated resulting in the rear droplet enveloping the front droplets. Shen et al. (2017) investigated fundamental flow characteristics of water-ethanol droplet suspended in sunflower oil merging in T-junction channel and rectangular microgroove, and splitting in two different microstructures i.e., cylinder obstruction and Y-junction bifurcation via micro-PIV technique. The microgroove generates higher probability for the coalescence of droplet compared to the T-junction in a microchannel. While, the junction of Y-shape can result in microdroplets splitting with a higher efficiency ($\eta > 95\%$) while keeping the microdroplet flow steady during the splitting at the junction. The existed studies focused on the different shape of the microchannels for droplet merging and splitting process, with less consideration given to the size or diameter of the microchannels (Darekar et al., 2017;

Kashid & Agar, 2007; Salim et al., 2008), which also one of the channel geometry's properties that can affect the flow characteristics of the droplets.

1.4 Scope of Study

The scopes of the overall studies are:

i. Design and fabrication of T-junction and offset T-junction microchannels using electric drill machine.

ii. Characterization of mixing performance of three dissimilar liquids i.e., propan-2-ol, water and sodium chloride solution inside T-junction and offset T-junction microchannels in the range of $5 \leq Re \leq 50$.

iii. Comparison and investigation of distilled water droplet behaviours suspended in food grade palm olein inside offset T-junction microchannel having different inlet and outlet radiuses i.e., 400 µm, 500 µm, 750 µm and 1000 µm via micro-PIV technique.

1.5 Hypothesis

i. For miscible mixing experiments, the mixing performance of these liquids for each Re is directly proportional to the mixing time, especially at low Re of 5, 10 and 20. This is because higher residence time inside the microchannel allows for higher molecular diffusion as the flow rate of the mixing liquids is low. As Re increases, massive convective diffusion dominates the flow which will influence the mixing process and performance.

ii. Viscosity-density difference contributes to the increases of mixing index as high viscous and more dense liquid pushes a low viscous and less dense liquid from the

channel wall which will result in an increase of the interface area and consequently improves the mixing in this regime.

iii. Diffusion process in immiscible liquids is relatively difficult to be characterized and compared with the miscible liquids due to chaotic advection. Hence, offset T-junction microchannel would offer better mixing performance for immiscible liquids due to the more space (indirect collision) and less momentum between the liquid-liquid interaction.

iv. The microchannel with smaller radius would have higher disperse phase's velocity than the channel with bigger radius. An increase in cross-sectional area and a decrease in disperse phase's velocity could be directly related to increased radius of offset T-junction microchannel.

v. The size of the droplets is getting bigger and may nearly equal to the microchannel's width as the radius of microchannel increases.

vi. The vector and velocity magnitude data of this droplet generation experiment should be in an agreement with Hagen-Poiseuille flow equation, which explains a minor increase in the channel's internal diameter results in a substantial increase in overall liquid flow.

1.6 Research Objectives

The main objective is investigation on mixing performance and droplet generation of dissimilar liquids. The specific objectives are:

i. To design and fabricate T-junction and offset T-junction microchannels;

ii. To characterize mixing index of dissimilar liquids inside T-junction and offset T-junction microchannels;

iii. To investigate the effect of offset T-junction microchannel's size on water-in-oil droplet's behaviours using micro-PIV technique.

1.7 Structure of Thesis

This thesis is classified into five main chapters, which are Introduction, Literature Review, Materials and Methods, Results and Discussion and lastly, Conclusion and Recommendations. Chapter 1 provides a general overview of this thesis, mainly on the background, problem statement, hypothesis as well as the objectives of the mentioned study. Chapter 2 highlights the details of the past studies that related to the microfluidic devices, which will breakdown into two main applications, micromixing and droplet generation. As for Chapter 3 Materials and Methods, all the experimental and analytical methods used in this study will be outlined in detail. The next chapter 4 will present all the findings as well as the discussion of the results of this microfluidics study. Finally, the last chapter, Conclusion and Recommendations contains a brief summary of the entire research work and recommended actions to improve this study.

CHAPTER 2

LITERATURE REVIEW

2.1 Chapter Overview

Chapter 2 provides a summary of literature studies related to microfluidic device application, mainly on microfluidic mixing and droplets generation processes that had been conducted in the past. The investigation method particularly on experimental study of both processes will be elaborated. The techniques used to characterize the mixing performance, and also the factors that influence the droplet behaviours will be discussed in Section 2.3 and 2.4, respectively. Performance of dissimilar liquid interaction is often described using various technical terms such as mixing, diffusion, reaction and dispersion. Mixing may be considered as a process that reduce the inhomogeneity between dissimilar liquids in order to bring them into contact with one another. Meanwhile, diffusion can be defined as a process where particles move and collide randomly from an area of high to low concentration. Reaction, on the other hand, is a product of mixing two or more substances. As for dispersion, it is a process where the particles spread out equally throughout a volume.

2.2 General Applications of Microfluidic Device

Microfluidic device is an instrument that deals with fluids at microscale level. This device has contributed significantly and extensively applied in biotechnology and environmental studies as well as in food and chemical industries due to their fast response time, low consumption of samples and high sensitivity.

For example, Pang et al. (2015) presented a new integrated microfluidic device for cancer cell separation based on cell size and deformability by merging the microstructure-

constricted filtration and pneumatic microvalves system. The issue arises when the filtration method for cell sorting is always limited by the variable hydrodynamic resistance of the filter due to cell build-up and clogging in the microstructures. Therefore, for each filter unit, two semi-circle and a rectangle, and the two side-by-side units formed a funnel-like shaped was designed to avoid cell damage and enhance the rate of separation. Meanwhile, the cell separation device consisted of a two-dimensional array of filtration constriction with eight group filter matrices for cell capture and sorting, and membrane microvalves were employed to control the flow across the filter matrices. The periodic sorting and release of cells using this proposed device considerably reduced cell accumulation and clogging, enhanced selectivity, and successfully separated cancer cells from the blood samples with more than 90% cell recovery and more than 80% purity. It demonstrated that this microfluidic system can offer a novel way to cancer cell separation with high collection recovery and purity.

Kuntaegowdanahalli et al. (2009) studied the principle of Dean-coupled inertial migration in spiral microfluidic device for separating different size of particles. This is because the use of porous membrane filter is not efficient at separating various size particles due to complex fabrication of 3D structures. Standard soft lithography method was used to fabricate five-loop spiral microchannel with two inlets and eight equally spaced outlets. Polystyrene particles of varying diameters i.e., 10 µm, 15 µm and 20 µm were used in the study, and all these particles come in one mixture. The flow description in the channel is based on Dean number, *De* which can be defined as:

$$De = Re\sqrt{\frac{D_h}{2R}} \qquad \text{Equation 2.1}$$

where *Re* is the Reynolds number, D_h is the hydraulic diameter of microchannel and *R* is the radius of convex surface's curvature. The microchannel successfully separated all the particles with efficiency of 90%. The study was furthered by demonstrating the application of their technique for separating neural cells, achieving 80% efficiency.

Wu et al. (2017) proposed a biomimetic artificial cilia-based microfluidic device to address both mixing and propulsion. It is essential to develop a microfluidic device that can perform multitasking for a wide range of applications. For instance, homogenous mixing and propulsion over the depth of the flow domain are required in drug delivery systems. The microfabrication process was used to create a rectangular microfluidic device with four straight microchannels and an array of artificial cilia implanted within one of the channel confinements. The experimental results showed that the proposed design had successfully achieved a maximum micromixing efficiency of 84% and flow rate of 0.089 µL/min. In short, this device can be utilised as a targeted drug delivery system that focuses on achieving a homogeneous mixture of the drug and its carrier prior to administration into target system.

Kim and Breuer (2007) introduced the use of bacterial carpets to enhance micromixing in a microfluidic device. This is because it is difficult to find a fluidic actuator to improve the mixing between parallel streams of fluids. Attachment of flagellated bacteria onto the solid surface can activate a solid-fluid interface, so that the cell and working fluid will be unmixed. 1 µm diameter and 2 µm long of Serratia marcescens were used in this study. For microfabrication, soft lithography technique was used to fabricate the fluid devices. The fabricated Y-junction microchannel consisted of two arms, and each arm carried fluid into a main mixing channel having dimension of 28 mm long, 15 µm high and 200 µm wide. It showed that the bacterial carpets could improve the mixing between

two streams in the microchannel. However, due to falling pH, which is affected by high carpet metabolism, the device performance decreased. Thus, bacterial carpet is still unsuitable to replace other conventional technique though it is robust and easy to manufacture.

Gelin et al. (2020) used a novel microfluidic system for high-throughput production of monodisperse droplets to experimentally evaluate the size of oil-in-water droplets. This is due to low production rate of microfluidic devices, which is still one of the key barriers to their widespread usage in industry. Hence, a three-dimensional (3D) emulsifier comprising four nozzles and a magnification of a droplet generator coupled to two inlets i.e., dispersed and continuous phases was developed. The experimental results showed a four folds increase in production throughput for the four nozzle chips while preserving strong monodispersity of the droplets. This proposed device can be scaled up for industrial applications that require far higher flow rates than microfluidic devices can generally provide.

2.3 Microfluidic Device for Micromixing Process

Micromixing process in microfluidic devices holds great importance in broad range of industrial applications i.e., biomedical, environmental and chemical industries. Mixing in microfluidic device aims to improve its performance particularly in achieving fast and complete mixing of different samples of fluids. This can be achieved by reducing its size i.e., shorter mixing channels and processing cost as it diminishes the consumption of specimens. Hence, in order to have better understanding of micromixing process in microfluidic device, the past studies of the microfluidic mixing by numerical and experimental methods done by numerous researchers will be presented in the following

sub-sections. The characterization of mixing performance also will be explained in Section 2.3.3.

2.3.1 Numerical Simulation of Micromixing

Chen et al. (2016) numerically studied species mixing performance of micromixers with serpentine microchannels. In order to achieve efficient mixing in a short length channel, the geometry of the micromixer plays dominant role to attain chaotic flow. The T-junction microchannels with three different structural design i.e., square-wave, multi-wave and zigzag at 4.7 mm from the junction were developed and their mixing performance were analysed for Re values in the range from 0.1 to 100. The microchannel with square-wave design was found more efficient compared to the multi-wave and zigzag, especially when Re is above 100, its mixing efficiency reached beyond 95% with a moderate pressure drop below 50 kPa due to its sharper turns and longer path of the flow. The simulation results demonstrated that the square-wave serpentine micromixer is effective, flexible when integrated to a microfluidic system.

Orsi et al. (2013) performed numerical study on the mixing behaviours of two miscible liquids systems i.e., water-water and water-ethanol in T-junction microchannel. There are few literatures devoted to study the mixing performance of two dissimilar liquids despite their importance in real microfluidic applications such as pharmaceutical, biomedical and biochemical processes i.e., nano-drugs preparation by antisolvent methods. The mixing process of two dissimilar miscible liquids systems was carried out in a microfluidic channel with Re ranging from 1 to 300 via a commercial CFD software. The numerical data showed the mixing performance of water-ethanol is slightly higher than that of the water-water system at $Re < 100$ due to high viscosity of ethanol and therefore lead to high residence time of the liquids occupying the interfacial region. On the contrary, at

high Re, water and ethanol streams were separated by a viscous layer that led to vortex formation and poor mixing performance.

Wang et al. (2002) enhanced the mixing of water and ethanol by placing obstacles in the Y-microchannel. The problem arises because of slow diffusion mixing process caused by laminar flow, and higher pressure drop due to the increase of channel length. In the study, theoretical analysis and commercial CFD software were used to analyse the mixing performance of the two liquids in a Y-micromixer. The findings show that by altering the flow pattern, obstacles can improve mixing performance, and the asymmetric placement of obstacles changes the flow directions and forces one fluid to flow into another, resulting in lateral mass transport (refer to Figure 2.1). Placing impediments in microchannels is a novel way for mixing in microfluidic devices, with the results providing significant information of the device's design.

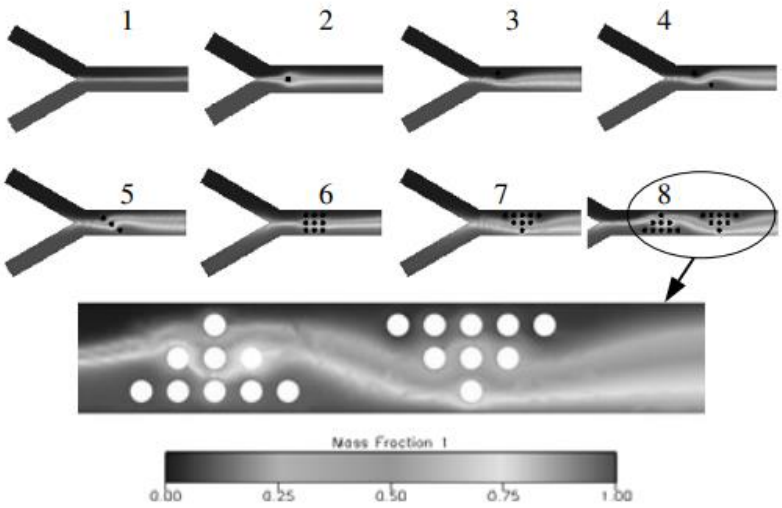

Figure 2.1: Evolution of design with obstacles in the Y-channel (Wang et al., 2002)

Ansari et al. (2010) numerically investigated the effect of water and ethanol stream interface's positions inside T-junction microchannels on the mixing index. This is because most of the existing works only focused at one position of the interface of the fluid streams and yet the optimum position where the mixing will be higher in the microchannel is left unknown. Therefore, a detailed mixing study at different interface positions was conducted inside T-junction microfluidic channel for varying Re. Various position of the interfaces showed significant variations in percentage of mixing at different Re. It was found that the interface's position in the channel for low $Re < 10$ had a major impact on mixing compared to the ones at higher $Re > 10$.

Solehati et al. (2014) enhanced the mixing quality of liquids in a micromixer by proposing T-junction microchannel with wavy structure. Two microchannels i.e., straight T-junction and T-junction with wavy structure were developed to compare their mixing index for Re ranging from 1 to 200. The numerical findings showed that T-junction microchannel with wavy structure performs better than a straight T-junction microchannel in terms of mixing, at higher Re of 200 (refer to Figure 2.2). This is due to the chaotic flow regime caused by the existence of periodically reversed secondary flow formed by curves wavy structure. The microchannel T-junction with wavy structure can be a popular choice in pharmaceutical and chemical industries, where both mixing efficiency and production efficiency are critical.

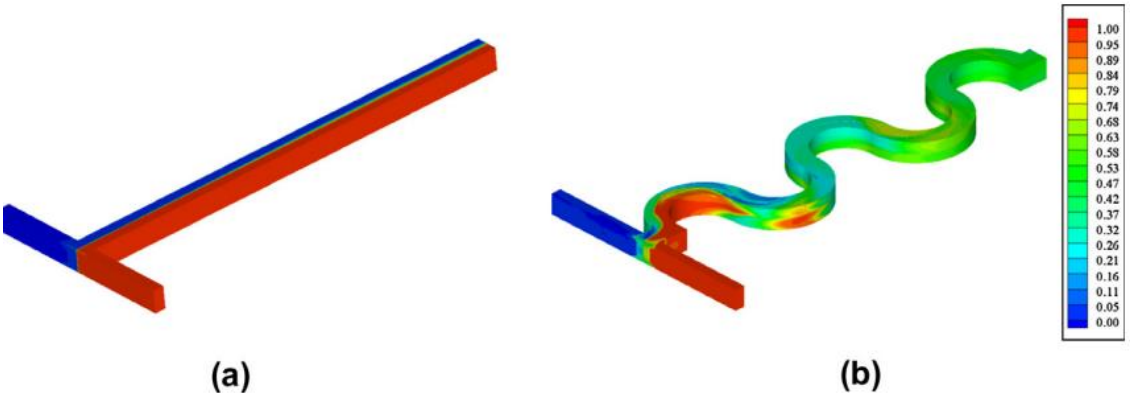

Figure 2.2: Mixing performance of micromixer T-junction designs for (a) conventional straight and (b) wavy structure at Re = 200 (Solehati et al., 2014)

Dundi et al. (2019) carried out numerical investigation to enhance liquid mixing at various Reynolds number ($0 < Re < 750$) using T-T microfluidic mixer. This is because the limitations and disadvantages of a simple passive T-junction microchannel found in the past studies i.e., poor mixing at low Re less than 200 (laminar regime) and high Re above 400 (pulsating vortex regime) (Dreher et al., 2009). Therefore, conventional T-junction microfluidic mixer was geometrically modified into T-T shaped with each inlet divided into two equal halves with a small gap difference. Mixing performance of T-T microfluidic mixer had shown a remarkable increase for both low and high Re due to hydrodynamic focusing effect and overlapping of vortices, respectively. T-T shaped passive microchannel is more capable in handling higher throughputs at lower pressure drop, hence it can perform better mixing over a wide range of Re compared to conventional T-junction micromixer.

2.3.2 Experimental Investigation of Micromixing

Shah et al. (2019a) experimented the effect of Y-junction microfluidic channel with different shape mixing units on mixing performance at $0 < Re \leq 100$. The problem arises because of the difficulty of microchannel with straight shaped design in achieving high

mixing efficiency due to slow molecular diffusion. Three designs which are Y-shaped circle split and recombination, Y-shaped rhombus-circle split and recombination and Y-shaped rhombus split and recombination were fabricated. It was found that mixing quality of Y-shaped rhombus-circle split and recombination microchannel is much better than the others, especially 99% efficiency at high Re of 80. The mixing improvement was majorly contributed by mixing units and sharp square bends which led to chaotic advection i.e., rotations and vortices.

Lin et al. (2011) experimentally evaluated the mixing of diluted sulphuric acid and a buffer solution (mixture of H_3BO_3, NaOH, KI and KIO_3) using Y-junction microchannel. The micromixer requirements for microchemical process application differ from the micro total analysis system in aspects of Re, pressure drop, material and fabrication process. Stainless steel Y-junction microchannel was fabricated via the lamination of functional layers with conventional machining and the microchemical liquids were experimented under Re range of 30 to 220. The mixing quality was evaluated based on a parallel-competitive reaction named Villermaux/Dushman reaction by Fournier et al. (1996), where the segregation index of this reaction was considered as the measure of the mixing quality of the micromixer. Improved mixing performance in the main channel can be attributed to its three-dimensional square-wave-shaped and periodic cubic grooves especially at higher flow rate in the range of $30 \leq Re \leq 220$.

Wang et al. (2011) experimentally investigate the mixing performance of DI water-glycerol solutions with viscosities ranging from 0.89 mPa·s to 50.76 mPa·s and total flow rates from 10 ml/h to 140 ml/h in a Y-junction microchannel. The problem arises when high mixing yield needs to be achieved for fast mixing liquids especially high viscous liquids with relatively high flow rates. The enhancement of the micromixing of DI water

and glycerol was done using acoustically induced bubbles at a working frequency range between 0.5 kHz to 3.5 kHz. A high mixing performance of 94% was achieved at viscosity of 5.69 mPa·s between 1 kHz and 2.5 kHz, while 78% performance at high viscosity of 44.75 mPa·s with driving frequency range reduced to 1.5 kHz – 2kHz. Due to the lack of bubbles inside the microchannel, poor mixing is seen for solutions with viscosities greater than 44.75 mPa·s across the whole operating frequency range. The interactions between the oscillating bubbles, acoustic actuation field, and the liquids help to improve mixing.

Dambrine et al. (2009) studied two dissimilar liquids having different viscosities in a Y-shaped microchannel with outlet dimension twice the size of inlets. Water and water/glycerol were used as working liquids and the cartographies of the concentration in glycerol were measured for different flow rates with a Raman confocal microscope equipped with an argon-ion laser. The outcome showed that the interdiffusion layer is not positioned at the center of the microchannel, and its average position evolved towards the transverse direction of the channel geometry during the mixing process. The displacement of the interdiffusion zone was affected by the conservation of the flow rate and of the concentration.

Wang et al. (2012) investigated the micro-mixing process in miscible liquids utilising two types of representative systems namely water-water (W-W) and water-ethanol (W-E) using micro-laser induced fluorescence (μ-LIF) technique. This is because the anti-solvent methods always involves both aqueous and organic solutions, which complicates the actual nano-drugs preparation in the pharmaceutical process. The mixing behaviour between these two mixing processes were observed under laminar flow conditions, ranging from 0.5 to 350 Reynolds number. Owing to the distinct concentration difference between two liquid streams as the effective driving force of mass transfer at the interface, the mixing

performance of water-ethanol is superior than water-water mixing. However, the two systems showed similar mixing performance with increasing Re because of enhanced convection. The study was furthered by demonstrating the nano-drugs preparation using anti-solvent precipitation process. As a result, smaller curcumin nano-precipitation may be accomplished in the microchannel at both low and high Re than at medium Re. This is consistent with the miscible water-ethanol system's measured mixing performance.

Lin et al. (2007) investigated mixing of ethanol and water in T-junction microchannel having J-shaped baffles (refer to Figure 2.3). This is due to the unsatisfactory T-junction microchannel's mixing performance found in the literatures. The mixing performances were obtained from the concentrations of the black ink in the fluid along the axial distance. The enhanced mixing was observed at the entrance of the main channel having J-shaped baffle that causes unequal lateral perturbation which increases the convection and molecular redistribution along the main channel. It was found the mixing increases with the increase of baffle number and Re.

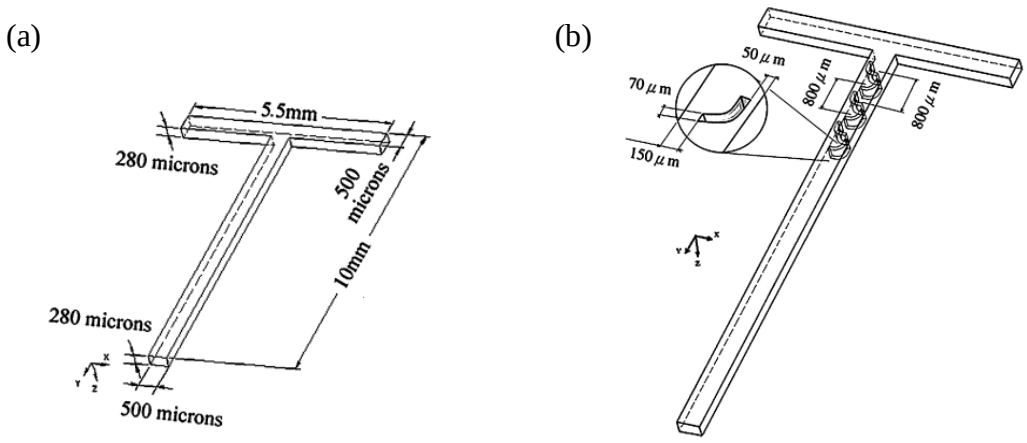

Figure 2.3: Schematic diagram of (a) T-micromixer, and (b) T-micromixer with six J-shaped baffles in the main channel (Lin et al., 2007)

Chung and Shih (2008) experimented mixing of ethanol and water using a planar micromixer with rhombic microchannels and a converging-diverging element. The problem arises because of the importance of turning angle for varies recirculation area which had not been discussed in their reference. The mixing efficiency was evaluated using image grey level, obtained from the concentration of deep blue ink dye that added to the ethanol for flow visualization. Result indicated that over 90% mixing can be achieved at 30° turning angle and Re ≥ 200. This proved that the rhombic micromixer has potential to be used in the future applications of fast and high throughput mixing.

Ansari et al. (2018) experimentally investigated the mixing performance of water-water in simple and vortex T-junction microchannels (refer to Figure 2.4) at Re ranging from 1 to 80. This is because a design modification of a simple T-junction microchannel need to be modified for an early development of the mixing which induces complex flow at lower Re. Hence, microfluidic T-junction channel with non-aligned inlet channels was fabricated to compare its mixing efficiency to the conventional design of T-channel. The experimental results showed that the mixing efficiency of liquids in the vortex T-junction micromixer is higher than in the conventional simple T-mixer, and is increasing with an increase Re. This vortex T-junction microfluidic channel is a promising design to efficiently increase mixing and can be applied to all type of micromixers.

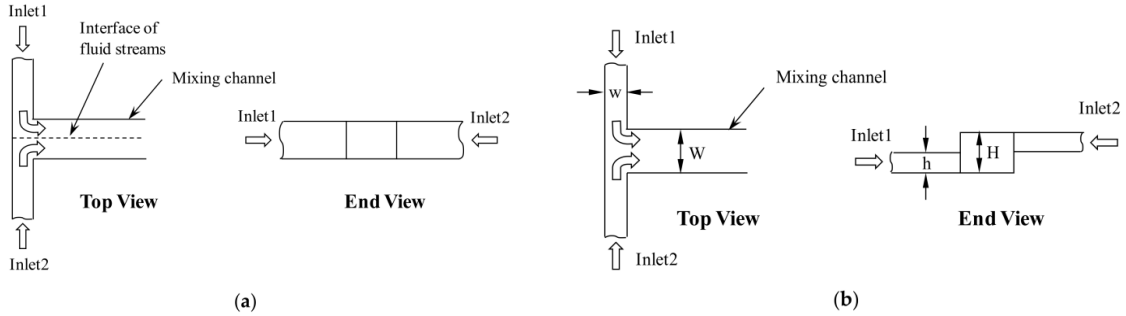

Figure 2.4: Schematic of the basic idea of the micromixer: (a) simple T-mixer and (b) vortex T-mixer.

2.3.3 Characterization of Micromixing Performance

There are several existing experimental techniques used for characterizing mixing and the related phenomena in both single and multiphase flows. According to Aubin et al. (2010), the efficiency of mixing in microfluidic devices i.e., chemical reaction, homogenisation, dispersion and emulsification holds a great significance as it will affect several process parameters such as process operating time, mass transfer rates as well as the product quality. In the case of single-phase liquid mixing, the mixing performance can be determined using a dilution-based method, either qualitatively utilising intensity of segregation or concentration homogeneity, or quantitatively where mixing time is deduced by determining the length necessary for visually-complete mixing. Meanwhile, for multiphase liquid-liquid mixing, dilution- and reaction-based technique is applied by monitoring the dilution of the organic dyes inside the mixture and calculating the mixing time from the grey scale levels in the images.

Fu et al. (2017) proposed mixing indices that take into account mean and dispersion information to increase the reliability of projected mixing performance. This is because the quantitative mixing index is calculated only on the basis of dispersion information extracted from intensity images, which provides relatively limited data due to the shift in average intensity as mixing improves. Two practical criteria i.e., reliability and repeatability precision were used to measure the efficiency of the quantitative mixing indexes. According to the results of the comparisons, the proposed approach can guarantee the accuracy of the computed result every time, with a repeatability precision less than 3.5 percent.

Zhang et al. (2019) experimentally investigated the effect of Rhodamine 6G and water flow regime on the mixing performance in the T-junction reactor using intensity of segregation (IOS) calculated by grey values via planar laser induced fluorescence (PLIF). The problem arises when there is some difference of mixing degree among the simulation works. In the study, the steady and unsteady engulfment flow at Re between 50 and 560 were chose to enhance the mixing performance due to increasing interface area of two streams. Result showed that steady engulfment flow at low Re improves mixing efficiency. On the other hand, unsteady engulfment flow occurred at $190 < Re < 380$ as the merged vortex passed through the channel, causing periodic oscillation in the chamber. The result of the large eddy simulation shows that the oscillation of vortex merging in the unsteady engulfment flow regime significantly enhance the mixing quality.

Mahmud and Tamrin (2020) improved the mixing index of water-water system in T-junction and Y-junction microchannels at various Re ranging from 5 to 100 by proposing new RGB colour model technique. The existing research is primarily based on intensity image dispersion (homogeneity) information, in which individual RGB values are first averaged before mixing index is calculated. This can eliminate over or underestimate of the calculated mixing index. The mixing index was computed by decoding each of the liquids present in the microfluidics according to their respective red R, green G and blue B. The result showed that T-junction microchannel has a slightly better mixing efficiency of 35% than that of Y-junction microchannel with 27.8% efficiency. This RGB colour model method is found robust, reliable and foreseen handy in characterizing mixing in real time for gradient mixing in microfluidic devices.

2.4 Microfluidic Device for Droplet Generation

Apart from micromixing process, the other important application of microfluidic devices is the generation of droplet with precise composition and size. This droplet formation widely used in microelectromechanical system (MEMS), microchemical technology, micrototal analysis system (μTAS) as well as in biotechnology applications. There are number of researchers experimentally conducted the bubble/droplet generation in microfluidic device via micro-PIV technique. The parameters i.e., viscosity, flow rate, interfacial tension, and diameter as well as the wall of the microfluidic channel that affecting the droplet behaviour will be discussed further in this section.

2.4.1 Investigation on Droplet Generation by Micro-PIV

Micro-PIV is a tool to measure flow velocity distribution, diffusion and mixing within a microfluidic device. Shen et al. (2017) investigated flow characteristics of water-ethanol droplet suspended in sunflower oil in T-junction with rectangular microgroove microchannel via micro-PIV technique. In order to understand the fluid dynamic characteristics of microdroplet merging and splitting processes, two sets of a combination of T-junction and rectangular microgroove were induced in two different microstructures i.e., cylinder obstruction and Y-junction bifurcation, respectively. Based on the results, for droplet merging, the microgroove has a higher microdroplets coalescence efficiency of 92% compared to 50% of that in a T-junction. Y-junction bifurcation, on the other hand, can split microdroplets with a high efficiency of more than 95% while maintaining microdroplet flow throughout the break-up process.

X. Wang et al. (2015) measured the internal flow field inside droplet during its formation process using micro-PIV technique. There are few studies concerning mass transfer in droplet generation process, eventhough knowing there is a strong impact

between the droplet's internal flow behaviour and the transfer process of the solute i.e., changes in interfacial properties of fluids. Water and butanol were used as dispersed phase and continuous phase, respectively. Both working fluids were experimented in a fabricated T-junction microchannel. The results indicated that both size and generation time of droplet decreased as the mass transfer rate increased due to the presence of internal circulation within the droplet during the formation process. By increasing the mass transfer rate, the vortex velocity inside the droplet can be lowered.

Oishi et al. (2011) measured the internal and surrounding flows of a moving droplet in a microfluidic device by developing a multicolour confocal micro-PIV system. This is because traditional micro-PIV could not see the interaction between two liquid phases because it was not designed to measure multiple phases and could not differentiate the tracer images of various phases. In the study, silicone oil as the continuous oil phase and a mixture of dilute water and glycerol as dispersed water phase were used as working liquids and were experimented in a PDMS-based T-junction microchannel. The results clearly demonstrated each phase's three-dimensional flow structure as well as the interaction between the interfaces. The multicolour confocal micro-PIV system also can be applied to chemical reacting flow and high shear flow applications.

Kinoshita et al. (2007) measured and visualized the internal flow of a moving water/glycerol-in-oil droplet in PDMS T-junction microchannel using confocal micro-PIV system. A confocal micro-PIV system was developed using a high-speed scanner and a simple Poiseuille flow to study the internal flow of a moving microdroplet. The out-of-focus light was successfully removed, and sharp high-contrast particle images were acquired inside a thin layer of a horizontal cross-sectional plane, allowing for the measurement of micro-flow velocity distributions in a 228 μm × 171 μm region with a

confocal depth of 1.88 μm. Due to the drag force on the contact surfaces with the surrounding walls of the microchannel, the liquid inside a moving droplet circulates intricately and three-dimensionally in a closed channel. The internal movement of a water/glycerol droplet improves mixing and speeds up any chemical reaction in the microfluidic device.

Jin and Yoo (2012) conducted flow visualization via micro-PIV to investigate water/glycerol-in-oil droplet merging processes in a Y-microchannel. The water/glycerol droplet-merging in oil was experimentally visualised inside two different Y-junction with straight and divergent microchannels. The droplets in the straight channel are limited by the channel walls, and the rear droplet penetrates the front droplet at the instant of coalescence, based on the instantaneous velocity vector fields in the scattered phase during the merging process data. In the divergent channel, on the other hand, a powerful vortex motion occurs as the rear droplet envelops the front droplet.

Liu et al. (2019) experimentally studied the internal flow field of droplets in a curved microchannel using a micro-PIV system. Compared to the straight channel, the internal flow characteristics of the droplet in the curved channel has less cognition despite its significance for microfluidic flow cytometry i.e., nanocrystal synthesis and cell manipulation applications. Glycerine aqueous solution (dispersed phase) and sunflower oil-hexadecane (continuous phase) were used and experimented in a T-junction channel with a bending unit at the outlet. With a capillary number ranging from 10^{-3} to 10^{-2}, a thicker oil film beneath droplets and a higher velocity across the water/oil interface resulted in the transition from four to three eddies inside droplets, and a similar pattern was observed when the viscosity ratio, droplet size, and channel curvature all decreased. When the size

of the droplet continuously decreased, the internal eddies inside droplets gradually approached and merged due to a smaller contact area between droplets and oil film.

2.4.2 Parameters Affecting Generated Droplet Behaviours

Numerous factors influence the behaviour of the generated droplet, including mechanical vibration, liquid viscosity, and channel features, such as surface, material, geometry and size.

Zhu et al. (2016) quantitatively characterized the formation of glycerol/water droplets in oil phase using a co-flow microchannel with mechanical vibration. The previous researchers successfully demonstrated the capability of mechanical vibration in controlling the droplet break-up process, however a comprehensive and quantitative study concerning the effects of vibration amplitude and frequency, fluid pressure and flow rate on droplet generation remains limited. In the synchronization region, where the frequency of droplet generation was synchronized with the vibration frequency, a wide range of droplet size was modulated, and the maximum synchronization frequency and minimum droplet size were characterized by approximating the fluctuating flow rate of glycerol/water phase. According to the results of the experiment, vibration can delay the formation of the jet and allow the dripping to occur at a wider range of flow rates. To summarize, vibration-modulated droplet generation in both dripping and jetting regimes allows for more efficient and precise droplet generation in practical applications.

Li et al. (2017) presented new open-channel microfluidic devices based on surfaces with patterned wettability that are efficient for water-in-oil emulsification. Because of the high flow rates required to maintain a stable emulsification interface within the channel, previous studies on droplet generation in open channel microfluidic devices were severely

limited. The localized incorporation of diverse surfaces with selective wettability, such as superomniphobic surfaces and surfaces that are both hydrophobic and oleophilic, enables the proposed open-channel device capability. The hydrophobic and oleophilic side walls and the open channels floor greatly improved the flow rate of continuous organic phase, in which enabled the emulsification of the aqueous phase, and prevented this dispersed phase from pinning on different areas of the microchannel. This research extends the capabilities of low-cost open channel microfluidic devices to generate hydrophilic microparticles for drug delivery, and potentially cell encapsulation in various polymers, both of which are highly wanted in the biological and biomedical fields.

Pang et al. (2014) studied the effect of microchannel's softness on the process of water-in-oil droplet formation for multiphase flows in a T-junction microfluidic device. As the measured liquid flow rate in the deformed channel is larger than those in the non-deforming channel at a given pressure difference, the soft wall in a microchannel can have a significant impact on the droplet break-up mechanism. A new T-junction microchannel was fabricated with one side of it has a thin PDMS layer that formed a flexible soft wall in which vibrates naturally while droplets are generated. When the droplets formed, the tensions at the liquid–liquid interface were briefly reduced due to the flexible wall, as opposed to drop formation in a constricted hard channel. As a result, the soft wall minimizes the droplet size's polydispersity.

Thurgood et al. (2019) used polydimethylsiloxane (PDMS) based microfluidic flow-focusing channel to investigate the size, gap and generation rate of oil-in-water and water-in-oil droplets. This is due to the influence of microfluidic structure's surface properties i.e., hydrophobicity of PDMS on the generation of stable droplets. The droplet generation characteristics were reversibly modified by exposing the channel to water for

48 hours and simply dried the channel with air for a long period. Generation of oil droplets in water occurred as a result of long-term exposure to water while the water-in-oil droplets production caused by the latter. The study successfully demonstrated the ability to generate the oil and also water droplets asynchronously and vary the gap between the successive droplets from a few hundred microns to a few microns in successive and rapid cycles.

Yao et al. (2019) investigated the effect of different viscosities of carrier oil on water-in-oil emulsion using a T-junction microchannel. Viscosity of the continuous phase is one of the dominant parameters affecting generation rate of droplets since it is highly related to capillary number that influence the break-up of droplet mechanism. Mineral oil with various viscosities and water were respectively used as continuous phase and dispersed phase in the microchannel. Due to high linear correlation of droplet generation rate and oil viscosity ($R^2 = 0.9979$) at ratio 3:4 of flow pressure between water and oil, this flow pressure parameter was set constant for all the experiments. The results showed that regardless of the flow pressure levels, the droplet size and droplet generation rate decreased as the oil viscosity increased.

Fu et al. (2009) experimentally investigated the gas bubble formation and break-up process in a microfluidic flow-focusing device at different flow rates for both phases and also viscosity for continuous phase using a high-speed micro-PIV technique. The size and geometry of microfluidic devices, flow rates and the fluid properties clearly controlled the bubble behaviours and their velocity, where their formation process happened very fast that even micro-PIV system having a slightly difficulty to quantify the features of the gaseous thread. The gas bubbles were generated in glycerol-water mixtures inside a 600 μm × 600 μm PMMA square microchannel. According to the findings, the collapse stage controls the majority of the bubble break-up process, with gas and liquid flow rates, as well as the

viscosity of the continuous liquid phase, influencing the thread neck collapse rate and time. The elongation and shear stress have a major contribution to the thread break-up in microfluidic devices rather than the capillary instability.

Liu et al. (2017) analysed the internal flow field of water-in-oil droplets inside a T-junction microchannel that mainly affected by viscosity ratio using micro-PIV method. Factors such as capillary number, viscosity ratio and interfacial tension that led to complex flow patterns, which not much considered by researchers. The experiments were conducted using different weightage ratio of dispersed phase (deionized water and glycerol aqueous mixture) that resulted in viscosity ratio and interfacial tension difference between dispersed phase and continuous oil phase. In comparison to the less viscous droplets, increased viscous dissipation resulted in the creation of extra circulations at a larger capillary number range inside the more viscous droplets. The flow pattern was discovered to be largely dependent on the capillary number, with the geometry of the droplet only affecting the axial and transverse velocity components values, as well as the flow behaviours inside intervals separated by the crucial capillary numbers.

Darekar et al. (2017) investigated the effects of diameter, flow rate, interfacial tension and channel wall's hydrophobicity on liquid-liquid multiphase flow patterns in Y-junction microchannels. Microchannels of two different diameters i.e., 260 µm and 760 µm, with and without hydrophobic coating for each channel were fabricated and used for water droplets in continuous organic phase i.e., butanol, butyl acetate and toluene experiments. Slug flow was discovered at low flow rates in both dispersed and continuous phases, and when the continuous phase flow rate was increased at a constant low flow rate in the dispersed phase, it changed to slug and droplet flow, then to droplet flow, before

changing to parallel flow when the dispersed phase flow rate was increased at a fixed low value of continuous phase flow rate. Flow pattern transitions were detected at lower flow rates as the microchannel diameter was reduced. Three flow patterns namely slug flow, slug and droplet flow, and droplet flow became more dominant as interfacial tension increased. Slug flow and other dispersed flow patterns became more prominent than parallel flow as the hydrophobic coating reduced wetting of the wall by the dispersed phase.

Deng et al. (2018) studied the terminal velocities of rising droplets i.e., soybean oil and toluene in quiescent water using co-flowing microfluidic device with various inner and outer diameter that affect the size of the droplet. Monodisperse microdroplets with controllable size ranging from 100 μm to 600 μm in co-flowing microchannels were prepared using soybean oil and toluene as dispersed phases and water as the continuous phase. For the same size droplet, the terminal velocity of toluene droplets is higher than the soybean oil droplets since toluene droplets have greater buoyance force due to their smaller density of 864.2 kg/m^3 compared to 917.5 kg/m^3 oil droplets. Their terminal velocity increased linearly with the increasing droplet diameter. The experimental results also reveal that a single microdroplet's terminal velocity is consistent with that of calculated rigid spherical particles of the same size and density, however a droplet swarm's terminal velocity is clearly higher than that of a single droplet.

2.5 Summary

In conclusion, there are two significant usages of microfluidic devices in this research work that will be studied, which are micromixing process and droplet generation. The applications of both processes have been presented in relevant section of this chapter. The micromixing process application covers both numerical and experimental of the existing studies. All the techniques used to characterize the mixing performance have their

own pros and cons. The droplet generation past studies including the experimentation via micro-PIV technique and the factors that influence the droplet behaviours have been highlighted as well in this chapter.

CHAPTER 3

MATERIALS AND METHODS

3.1 Chapter Overview

This chapter covers the microchannel fabrication, experimental setup and also the method used to characterize mixing performance of dissimilar liquids and droplet generation in T-junction microfluidic channel (Figure 3.1).

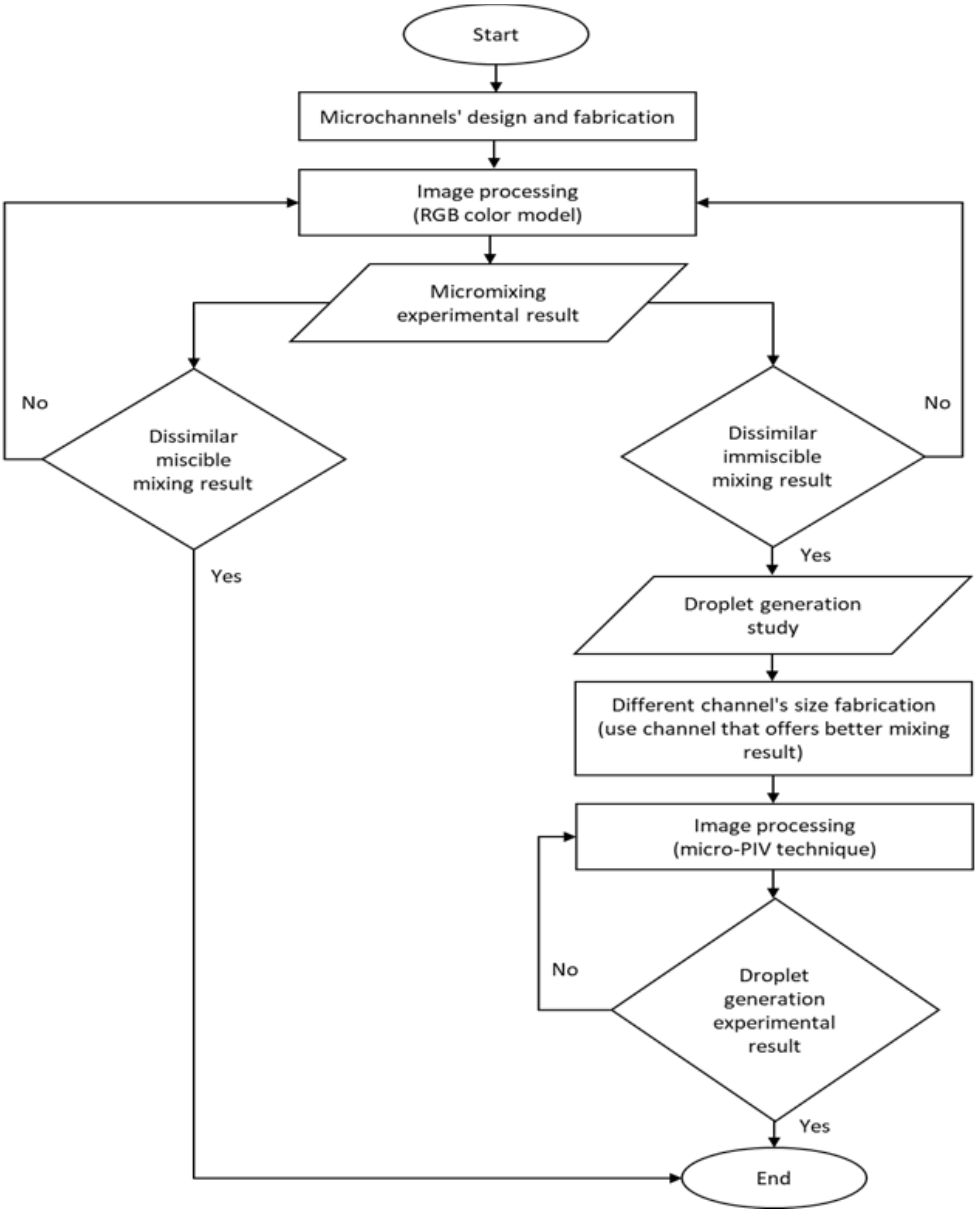

Figure 3.1: Flowchart of the methodology

3.2 Fabrication of Microfluidic Channel

The first iteration of the fabricated T-junction microchannel consists of a laminated film with an average thickness of 250 µm that was sandwiched between poly (methyl methacrylate) (PMMA) sheet and another laminated film with double-sided adhesive sheets. However, propan-2-ol dissolved the adhesive from the double-sided adhesive sheets and cause leakage in the fabricated microchannel.

Figure 3.2 shows the final version of the fabricated T-junction and offset T-junction microchannels for micromixing experiment. Two units of PMMA with thickness of 8 mm were cut using a 40 W CO_2 laser (Figure 3.3) to produce microchannel with an overall dimension of 20 mm length and 17 mm height. To remove dust, all the layers were cleaned using clean-room tissue. Then, the PMMA were drilled using drill press machine to form the microchannel shape with inlets and outlet radius of 750 µm. Finally, the top end of the outlet port was sealed flushed with the wall using epoxy to avoid the liquids overflow to the top.

The fabricated offset T-junction microchannel for droplet generation experiment is shown in Figure 3.4. The experiment used four units of laser-cut PMMA having overall dimension of 25 mm length, 20 mm height and 6 mm width. The sheets were drilled using electric mini drill to form offset T-junction microchannel shape with inlets and outlet radius of 400 µm, 500 µm, 750 µm and 1000 µm.

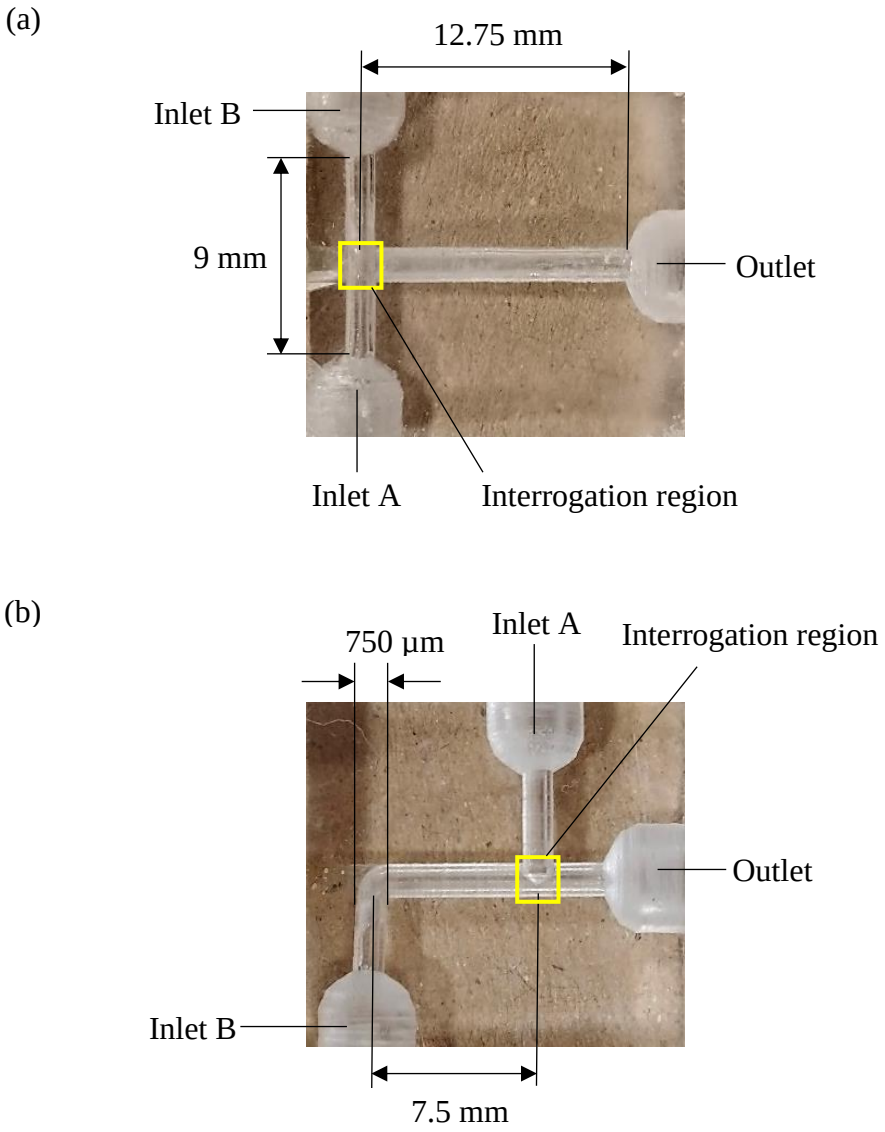

Figure 3.2: Fabricated (a) T-junction and (b) offset T-junction microchannels with inlets and outlet radius of 750 µm for micromixing experiment

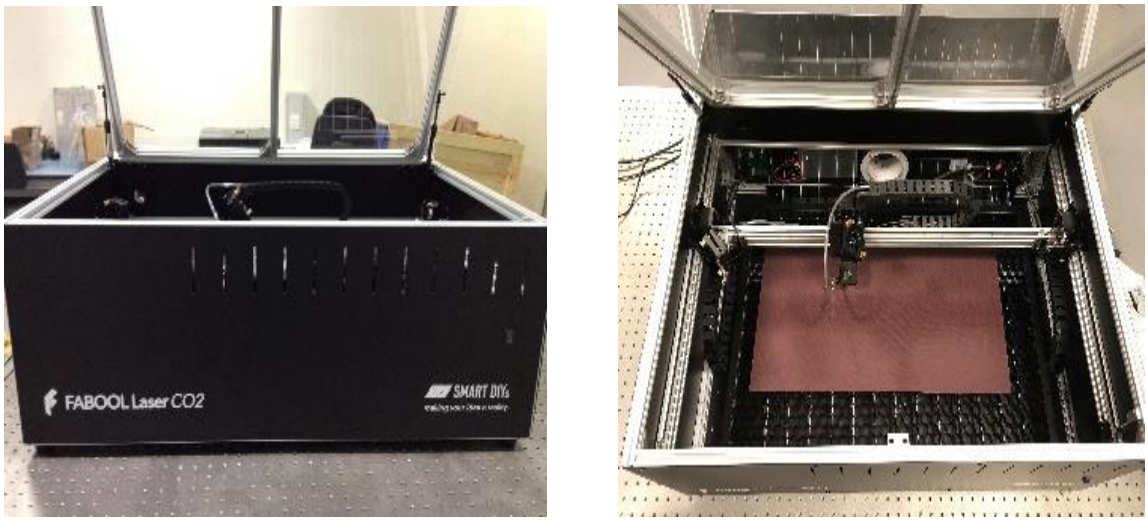

Figure 3.3: CO_2 FABOOL Laser Mini

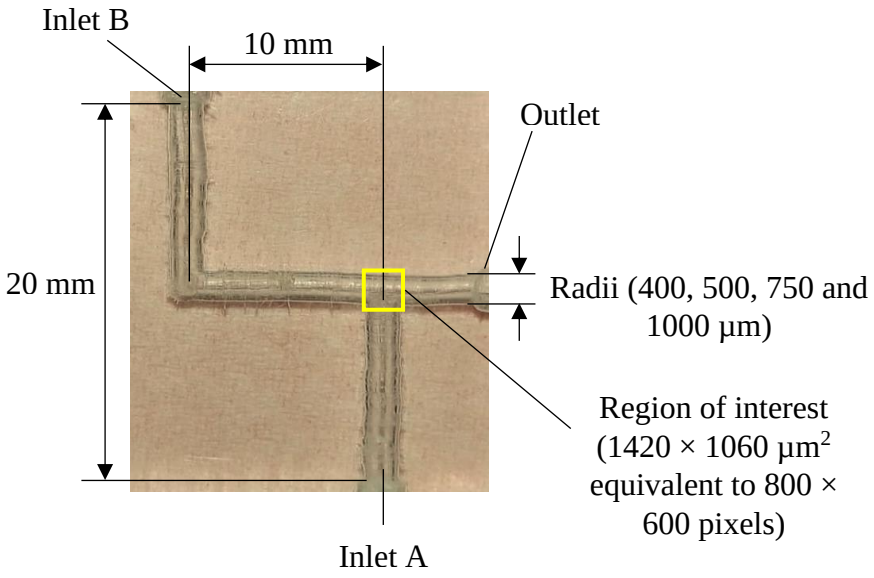

Figure 3.4: Fabricated offset T-junction microchannel with different inlet and outlet radiuses i.e., 400 µm, 500 µm, 750 µm and 1000 µm for droplet generation experiment

3.3 Experimental Setup for Micromixing

Figure 3.5 shows an experimental setup comprising of fluid driving mechanism, a microfluidic channel and optical imaging system. Both syringes containing dissimilar liquids of coloured solutions with a nominal capacity of 10 mL and volumetric tolerance amounts to ± 4% at room temperature are connected to a lead screw actuated by a two-phase stepper motor (NEMA 17). The stepper motor is controlled by Arduino Uno microcontroller and powered by linear DC power supply (Model: GPS-3030D, Good Will Instrument Co., Ltd). This syringe pump as well as microcontroller and electronic hardware were developed by Mahmud and Tamrin (2020). It is noted that the syringe pump was fabricated in-house and therefore was not calibrated and benchmarked to the industry standard. The resolution of the stepper motor used for the experimentation was increased from 150 to 1800 steps per rotation using A4988 motor driver. A digital video microscope (Model: MD500, AmScope) with 4× magnification was used to capture 1280×720 pixels resolution of mixing images in microfluidic channel. It is noted that the mixing time for each frame captured is 0.125 s (8 frames per second). In addition, the maximum frame rate that can be captured is limited by the installed CCD camera used in the microscope. The whole measurements and experiments were carried out at room temperature 25 ± 1 °C under atmospheric pressure. The settings of the ambient lighting and microscope were also kept constant. Using MATLAB code, the mixing index is quantified using image processing which will be described in Section 3.3.1.

The liquids that were injected into inlet A and inlet B for three different mixing experiments were shown in Table 3.1. Each blue and yellow food grade dyes was mixed with the chosen liquids with ratio of 1:100 for each mixing experiment. The food dye

solution used for the experiment was assumed to have the same density and dynamic viscosity as of water (Mahmud & Tamrin, 2020; Viktorov et al., 2016).

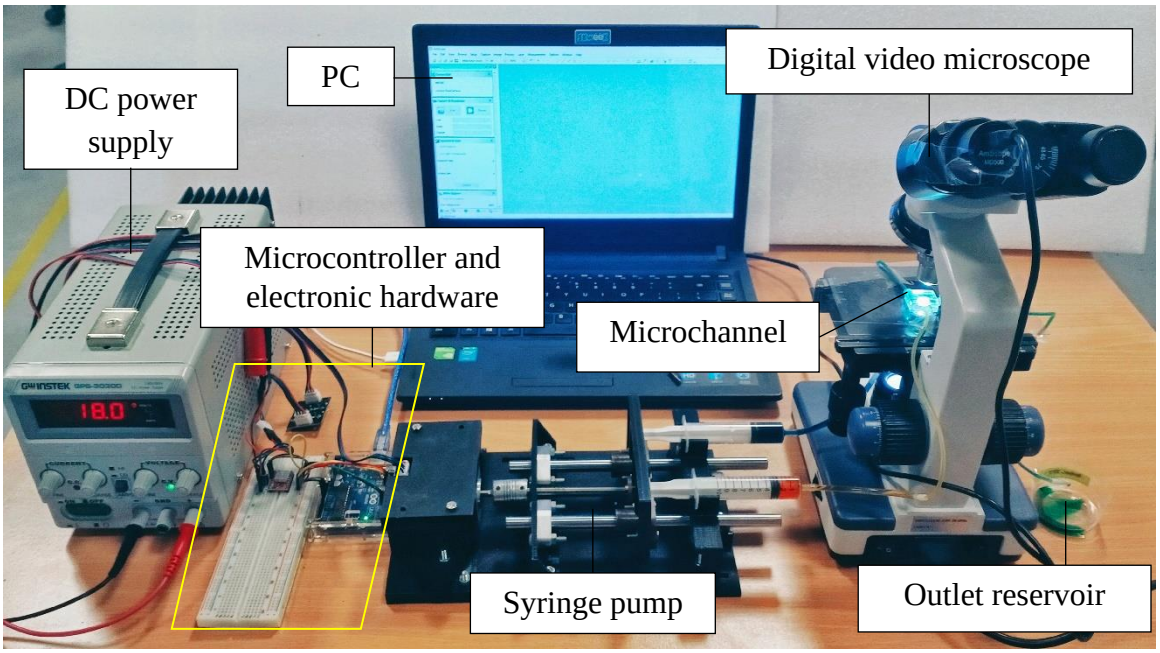

Figure 3.5: Experimental setup

Table 3.1: Dissimilar liquids for micromixing experiment

Experiment	Inlet A	Inlet B	Miscibility
1	Propan-2-ol + blue dye	Water + yellow dye	Miscible
2	Water + yellow dye	Sodium chloride solution + blue dye	Miscible
3	Propan-2-ol + blue dye	Sodium chloride solution + yellow dye	Immiscible

Since during the processes of mixing, the density as well as viscosity of the mixture were different, the properties of water were taken as the reference for the whole experiments (Wang et al., 2012) to calculate the flow rate, motor step for the syringe

pump's operation and evaluation of mixing performances. The volume flow rate, Q (m^3/s) is defined as:

$$Q = \frac{Re \times \mu \times A}{\rho \times D} \quad \text{Equation 3.1}$$

where Re is Reynolds number (5, 10, 20, 30, 40, 50), μ is the dynamic viscosity of water (8.9×10^{-4} Pa·s), A is area of channel (1.8×10^{-6} m^2), ρ is the density of water (997 kg/m^3) and D is the diameter of the channel (1.5×10^{-3} m).

3.3.1 Micromixing Characterization by RGB Colour Model

Generally, the image intensity is used to find the mixing performance based on the dispersion/homogeneity (Chen et al., 2016; Fu et al., 2017), however such an estimate can result in over and/or under estimate of the mixing index (Mahmud & Tamrin, 2020). For this reason, RGB colour model is employed for micromixing characterization by decoding each of the mixing images in which the respective intensities in red, green and blue colour pixels can be found using the following equation (Mahmud & Tamrin, 2020):

$$Mixing\ Index = \frac{N_{mixed}}{N_{mixed} + N_{unmixed}} \quad \text{Equation 3.2}$$

where N_{mixed} and $N_{unmixed}$ are the number of pixels classified as mixed and unmixed solution, respectively, based on the following:

$$N_{mixed} = n(\{r_{g,min} \leq R \leq r_{g,max} \cap g_{g,min} \leq G \leq g_{g,max} \cap b_{g,min} \leq B \leq b_{g,max}\}) \quad \text{Equation 3.3}$$

and

$$N_{unmixed} = n(\{r_{b,min} \leq R \leq r_{b,max} \cap g_{b,min} \leq G \leq g_{b,max} \cap b_{b,min} \leq B \leq b_{b,max}\}) + n(\{r_{y,min} \leq R \leq r_{y,max} \cap g_{y,min} \leq G \leq g_{y,max} \cap b_{y,min} \leq B \leq b_{y,max}\}) \quad \text{Equation 3.4}$$

where the number of pixels, satisfying RGB conditions, is specified using n while $\cap$ symbolizes for the Boolean AND operation. The letters $'r'$, $'g'$ and $'b'$ are used to identify the red, green and blue values respectively. The letters in the subscripts (g, b and y) denote the respective intensity values of the RGB for green, blue and yellow pixels. Their values range between 0 (unmixed solution) to 1 (fully mixed solution).

3.4 Experimental Setup for Droplet Generation and Micro-PIV Processing

The droplet generation experimentation schematic diagram is shown in Figure 3.6, including microfluidic channel and the associated optical imaging measurement system along with fluid driving mechanism. The droplet behaviours focused at the junction of microfluidic channel were captured using similar model and magnification of microscope used in micromixing having resolution of 800×600 pixels. It is noted that the minimum time step allowable is 0.0455 s (22 frames per second). The fluid driving mechanism consisting syringe pump, microcontroller and electronic hardware have already been described in Section 3.3. The input parameter setting maintained for all the experiments including setting of microscope and initial flow rate was summarized in Table 3.2.

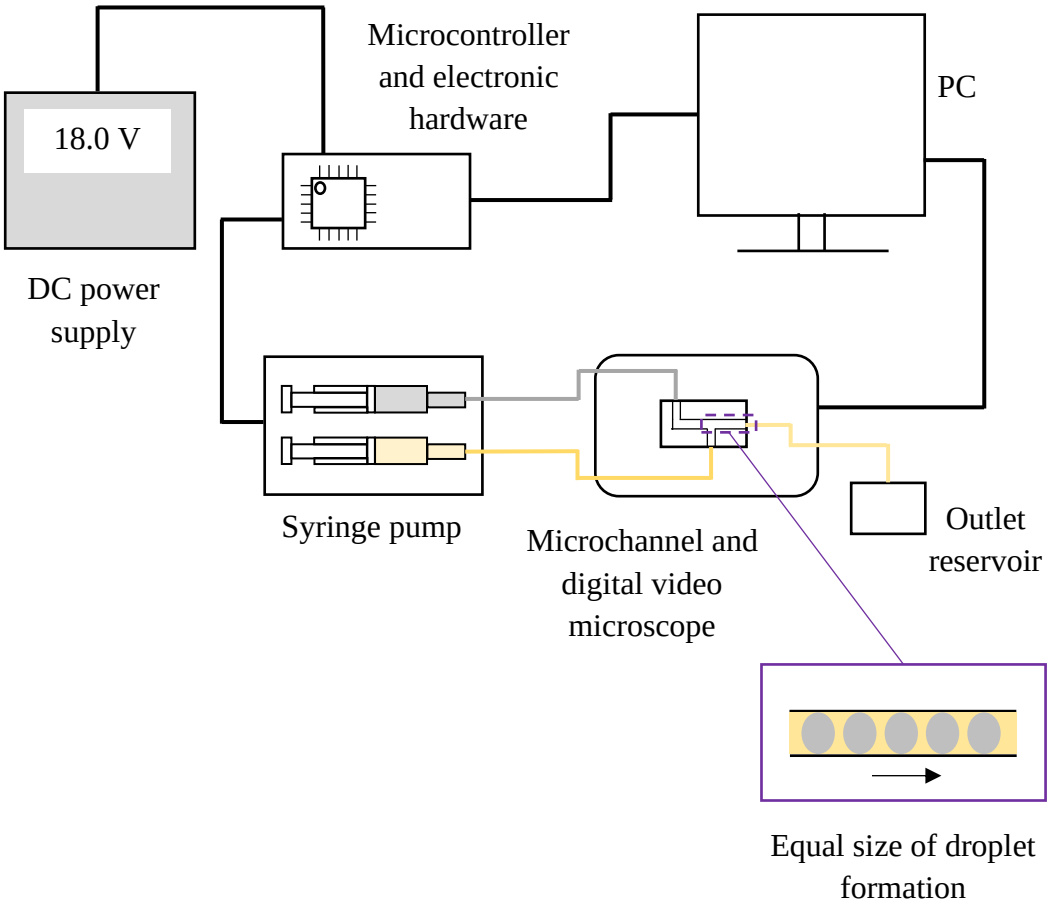

Figure 3.6: Schematic diagram of the experimental setup for droplet generation

Table 3.2: Controlled parameters for micromixing experiment

Parameter	Value
Exposure time	3.906 ms
Frame rate	21.8 fps
Resolution	800 × 600 pixels
Motor step	5
Flow rate of liquid at the inlets	0.16 mm^3/s

The experiment originally used the Magnaglo® 14A fluorescent magnetic powder (mean particle size of 6 µm, manufactured by Magnaflux) suspended in Carrier II (density of 802.837 kg/m^3, dynamic viscosity of 0.0026 Pa·s at 38°C, manufactured by Magnaflux) as dispersed phase, however due to its fast settling in the oil, the preliminary experiments were unsuccessful.

Hence, food grade palm olein having a density of 917 kg/m^3 and viscosity of 7.97 × 10^{-2} Pa·s (Siddique et al., 2010) and distilled water (density of 997 kg/m^3, viscosity of 8.90 × 10^{-4} Pa·s) seeded with polystyrene microspheres particles (manufactured by Thermo Scientific™ 4210A) were respectively injected into inlet A and inlet B for different diameters of offset T-junction microchannels. Food grade palm olein was chosen for this study because it is one of the most commonly used oil in household and food industry (Idris et al., 2018) and also has high stability index (Idris et al., 2018) in the emulsification process. The seeding particles (Table 3.3) was mixed with distilled water with ratio of 1:4 for each experiment. The food grade palm olein and the seeding particles were assumed to have the same density and dynamic viscosity as distilled water. These particles do not affect the palm olein because they are suspended in water. Due to the particles small size and minimal density difference between the particles (1050 kg/m3) and water (997 kg/m3), they are assumed to faithfully follow the flow of water (Santiago et al., 1998; Tamrin et al., 2015b).

Table 3.3: Specification of seeding particle (Turner et al., 2018)

Composition/ Material	Polystyrene
Diameter	10 μm ± 0.08 μm
Concentration	0.2% solids
Density	1.05 g/cm^3
Refractive index	1.59 at 589 nm (25°C)

By adopting time-resolved as the image sequencing style in micro-PIV for MATLAB software (Thielicke, 2014; Thielicke & Stamhuis, 2014), the flow patterns of the fluids were obtained. The region of interest was set to the whole area of the 800×600 pixels frame. The physical dimension of the region is 1420×1060 μm^2 (see Figure 3.3). Therefore, the resolution is 1.77 μm × 1.77 μm per pixel, respectively. For image pre-processing, contrast limited adaptive histogram equalization (CLAHE) was applied to the images for visibility enhancement (Yadav et al., 2014). It is noted that the average seeding density is 5 particles per 32×32 window while the threshold parameter for the signal-to-noise ratio was set at 1.5. The spatial resolution is defined by the size of the window of the interrogation spot and out-of-plane resolution (Meinhart et al., 1999). In the case of volume illumination, the depth of focus of the microscope objective defines the measurement region (Meinhart et al., 2000). By overlapping the interrogation spots with 50%, the resulting velocity fields have a spatial resolution of 28.4 μm × 28.4 μm × 55.5 μm. Then, the images were processed by cross-correlation function in order to obtain the raw velocity vectors of the liquids. To compensate for aberration (Tamrin et al., 2015a, 2015b), the calibration was performed using the image of 10 μm polystyrene microsphere flowing inside the microchannel, which resulted to 6×6 pixels based on 4× magnification of digital

video microscope. The vector validation was done to eliminate some incorrect vectors remaining from noise peaks in the correlation function.

3.5 Summary

As a summary, this chapter presented methodology used in the entire research work. The fabrication of microfluidic channels, experimental setup and also the technique used to conduct micromixing and droplet generation experiments have been discussed in detail in each section of this chapter.

CHAPTER 4

RESULTS AND DISCUSSION

4.1 Chapter Overview

The first part of Chapter 4 discusses experimental result pertaining to micromixing experiment, while the latter elucidates experimental result of droplet generation experiment.

4.2 Micromixing Results

The effect of channel's design on the mixing index of two dissimilar miscible liquids will be discussed in Section 4.2.1 and 4.2.2, while for immiscible liquids will be explained in Section 4.2.3. A better channel's design in Section 4.2.3, either T-junction or offset T-junction microchannel will be used in droplet generation studies.

4.2.1 Effect of Channel's Design on The Mixing Index of Two Dissimilar Miscible Liquids (Propan-2-ol and Water)

For propan-2-ol and water mixing in T-junction microchannel, the graph (Figure 4.1(a)) indicates that as mixing time for each Re increases, mixing index also increases until maximum index of 1 is reached. At the early stage of mixing, Re of 10 shows a steep rising index than the others. This is because higher molecular diffusion takes place while the flow rate is low due to its higher residence time (Mondal et al., 2018). Figure 4.2(a) shows that propan-2-ol and water do not flow side by side in the low Re regime as there is a large amount of mass transfer perpendicular to the main flow (Wang et al., 2012). At Re = 5, it can be seen that the mixing process is slower to take effect at the early stage but as the diffusion time increases, the mixing quality of propan-2-ol and water also increases. However, at Re = 30, the less residence time for diffusion transport results in poor mixing

performance at a fixed position (Wang et al., 2012), which can be observed from 0 to 0.375 s. Meanwhile, at high Re of 40 and 50, maximum index of 1 is reached in the shortest time at 0.25 s. The process is dominated by massive convection process which is occurred when stratified flow changed to vortex flow (Wang et al., 2012). With the increase of Re, the momentum also increases resulting in circulation in wider regions of flow and produced a local maximum velocity (Chung & Shih, 2008) from 3 mm/s (Re = 5) to 29.8 mm/s (Re = 50). The effect of induced circulation results in efficient mixing of propan-2-ol with water as the circulation provides further increased interfacial area as well as better advection (Chung & Shih, 2008). The efficiency of mixing then remains at 100%. The experimental results of propan-2-ol and water mixing in the T-junction microchannel are much similar to the reported experimental result of Wang et al. (2012), where ethanol and water are being experimented in the T-junction microchannel.

(a)

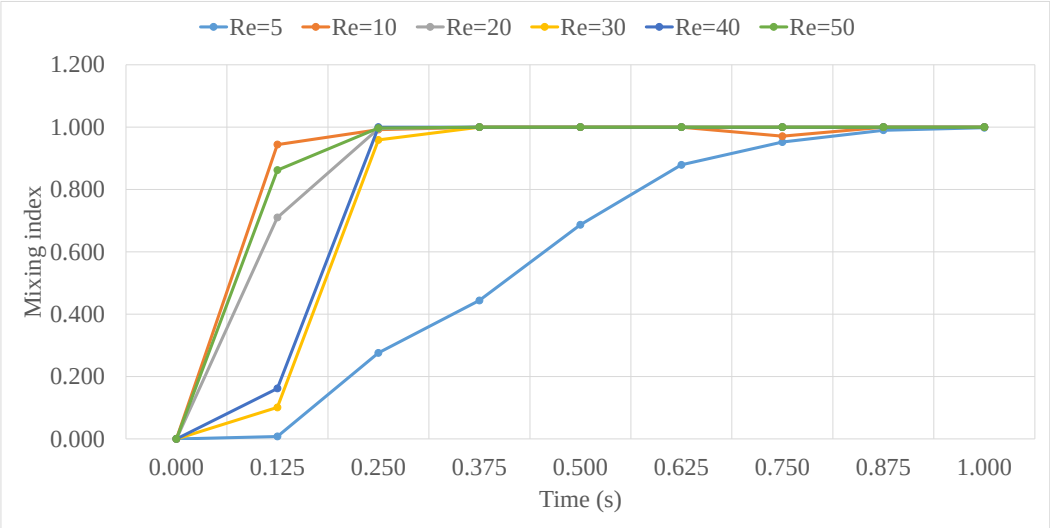

(b)

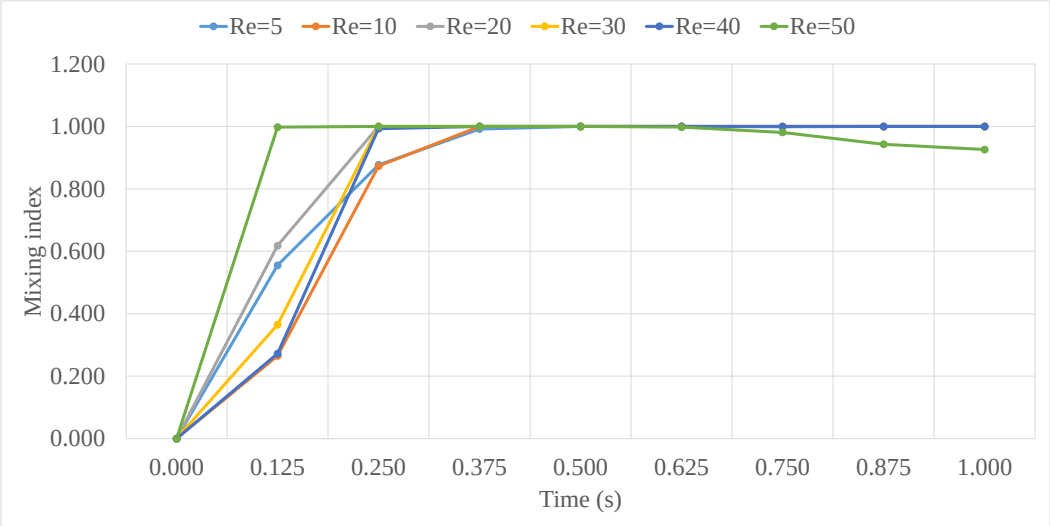

Figure 4.1: Mixing index of propan-2-ol and water at (a) T-junction, and (b) offset T-junction

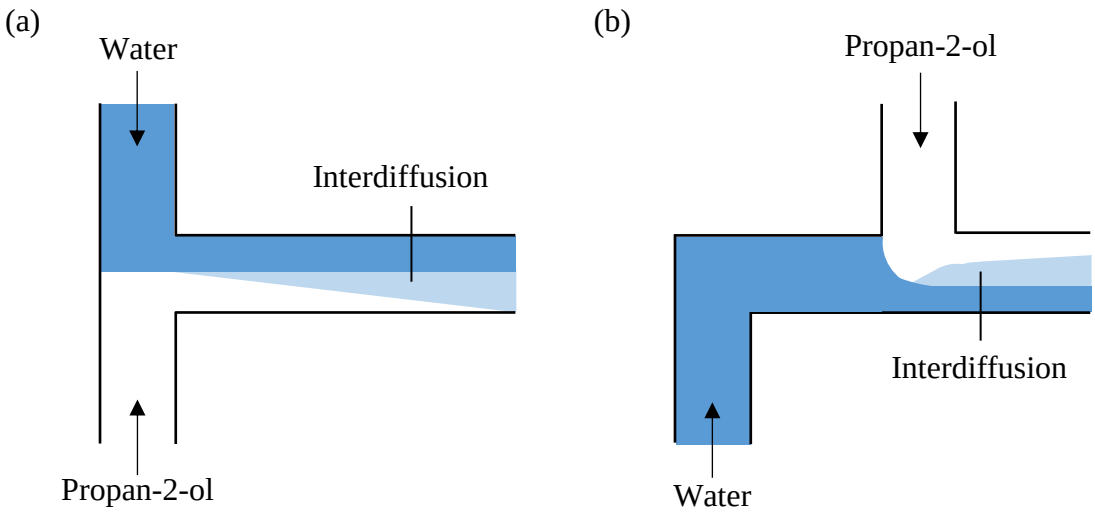

Figure 4.2: Top view indicating schematically the interdiffusion layer of miscible propan-2-ol-water micromixing in (a) T-junction and (b) offset T-junction microchannels

Based on Figure 4.1(b), the graph of mixing in offset T-junction microchannel has the same pattern with the ones in the T-junction microchannel, where mixing index increases with the mixing time for each Re. At low Re of 5 and 20, propan-2-ol diffuses into water quickly due to the concentration difference for liquid-liquid mass transfer (Wang et al., 2012). For medium Re of 30, the mixing performance at the early stage of mixing is found similar to the previous propan-2-ol and water experiment in T-junction microchannel. At high Re, the experimental results of propan-2-ol and water mixing within offset T-junction microchannel is fitted the explanation of reported experimental result of Wang et al. (2012), where ethanol and water are being experimented in the offset T-junction microchannel. The propan-2-ol stream is pushed to the center of the channel owing to its inertia while the water stream is moved towards the walls of the channel in the premises of the convergent junction of the two flow inlets (Wang et al., 2012) as illustrated in Figure 4.2(b). At Re = 50, mixing index increases and after half second, it starts to decline. Nevertheless, the highest mixing index of 1 is fastly achieved at this Re around

0.25 s. This is because at high Re, the interfacial area between propan-2-ol and water increases due to high liquids velocity. As a result, the convective diffusion compared to molecular diffusion, owing to the liquid lamellae stretching and subsequent thinning (Wang et al., 2012), dominates the mixing process.

4.2.2 Effect of Channel's Design on The Mixing Index of Two Dissimilar Miscible Liquids (Water and Sodium Chloride Solution)

Figure 4.3(a) illustrates mixing index of water and sodium chloride solution is directly proportional to the mixing time for each Re in T-junction microchannel. At the same early stage of mixing around 0.125 s to 0.375 s, the mixing index values increase as Re increases. The result of rising the Re at the T-junction of the microchannel is the generation of vortices at junction (Ansari et al., 2018). This vortex generation stretches and increases the interface area of the two streams. At the same time, the factor of viscosity and density difference starts to show its impact. Sodium chloride solution with a higher viscosity and density pushes the less viscous and less dense water from the channel walls and somewhat envelops it (Lobasov et al., 2016) as shown in Figure 4.4(a). This resulted in an increase of the interface area of miscible liquids and consequently enhance the mixing in this regime (Lobasov et al., 2016). Unlike previous experiment of propan-2-ol and water mixing process, especially at low Re of 5, it can be seen that the liquids are not yet fully mixed at 1 s due to the very slow molecular diffusion. A well-mixed state for this Re can be achieved after a long enough mixing time (Wang et al., 2012).

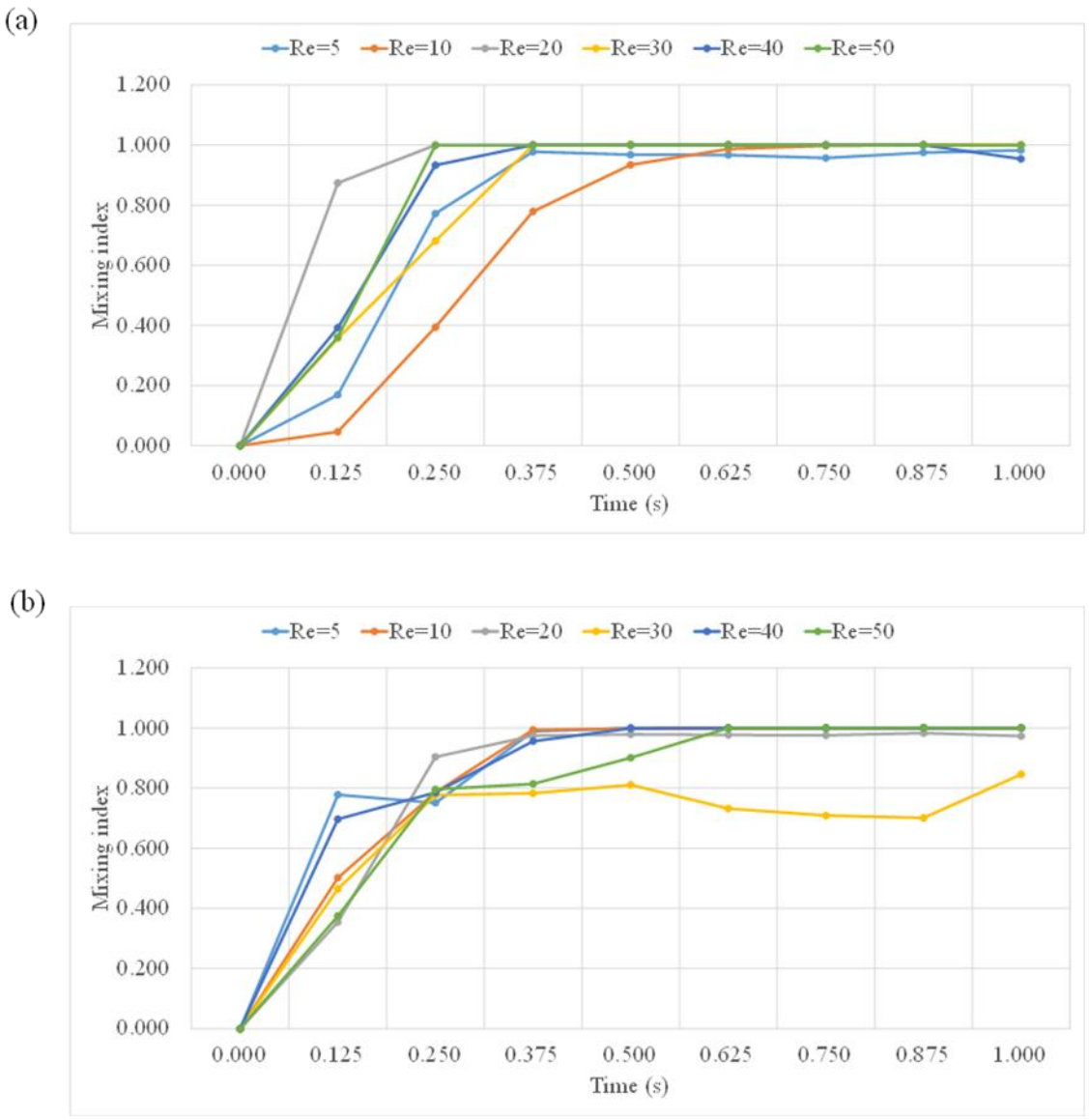

Figure 4.3: Mixing index of water and sodium chloride solution at (a) T-junction, and (b) offset T-junction

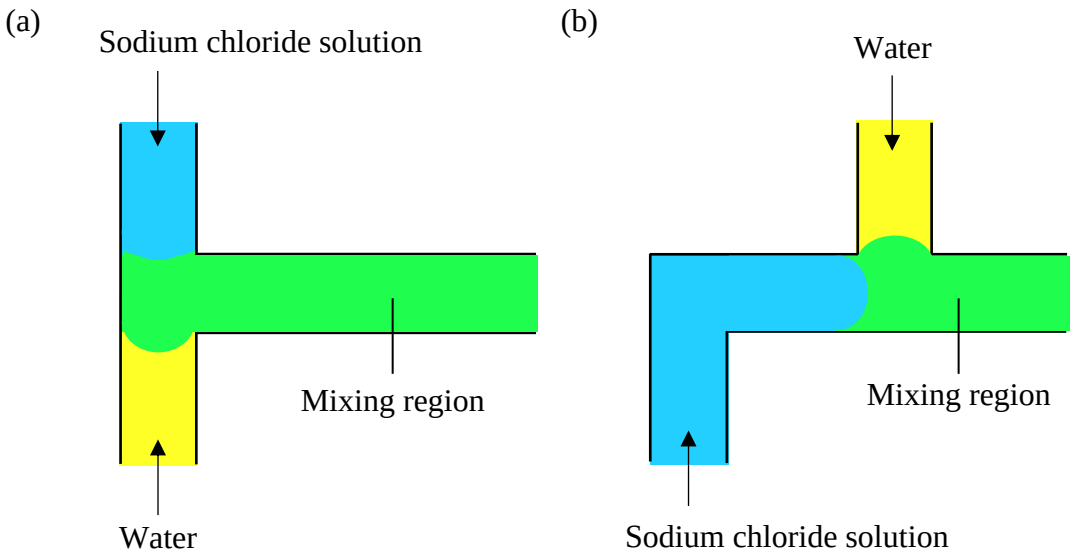

Figure 4.4: The schematic diagram mixing of water and sodium chloride solution in (a) T-junction, and (b) offset T-junction microchannels

Meanwhile, for offset T-junction microchannel, mixing index dropped at 0.5 s then rose again at 1 s at medium Re of 30 shown in Figure 4.3(b). Compared to previous mixing experiment of same liquids in T-junction microchannel, very poor mixing between water and sodium chloride solution can be observed at this medium range of Re. With the increasing values of Re, the residence mixing time is lowered and enhanced inertial effects lead to decrease in mixing performance of water and sodium chloride solution (Wang et al., 2012) from Re = 5 to Re = 30. On the other hand, at high Re of 40 and 50, the mixing index increases due to the transition of the flow pattern, which is from stratified to vortex flow (Wang et al., 2012). At low as well as high values of Re, the mixing performances are better in comparison to medium Re. At high Re, the mixing performance is good due to the massive convection caused by the effect of stretching and thinning of liquid lamellae and

wrapping of two liquid lamellae yield and enlarged the interfacial surface area (Wang et al., 2012) as shown in Figure 4.4(b).

4.2.3 Effect of Channel's Design on The Mixing Index of Two Dissimilar Immiscible Liquids (Propan-2-ol and Sodium Chloride Solution)

Based on Figure 4.5(a), a zig-zag graph pattern can be seen when propan-2-ol mixed with sodium chloride solution in T-junction microchannel. At low Re of 5, 10 and 20, as time increases, mixing index also increases but after 0.25 s, the values for Re = 10 and Re = 20 drop and then rise again. Meanwhile, at medium and high Re of 30, 40 and 50, the mixing index keeps fluctuating as it drops and rise repetitively. In fact, the molecular diffusion process between immiscible propan-2-ol and sodium chloride solution is difficult compared to the previous two miscible mixing experiments. Because of the fact that the salt ions are smaller in size, water molecules displace the alcohol molecules in solvating these ions (Fang et al., 2018). The molecular attraction between salt ions and water molecules is much stronger compared to alcohol owing to the fact that alcohol is less polar than its counterpart. This results in formation of bonds between all of the water molecules and salt ions, resultantly providing no opportunity to form hydrogen bonds with the alcohol (Fang et al., 2018). As a result, the water-salt solution becomes immiscible with propan-2-ol and thus forms a separate layer.

(a)

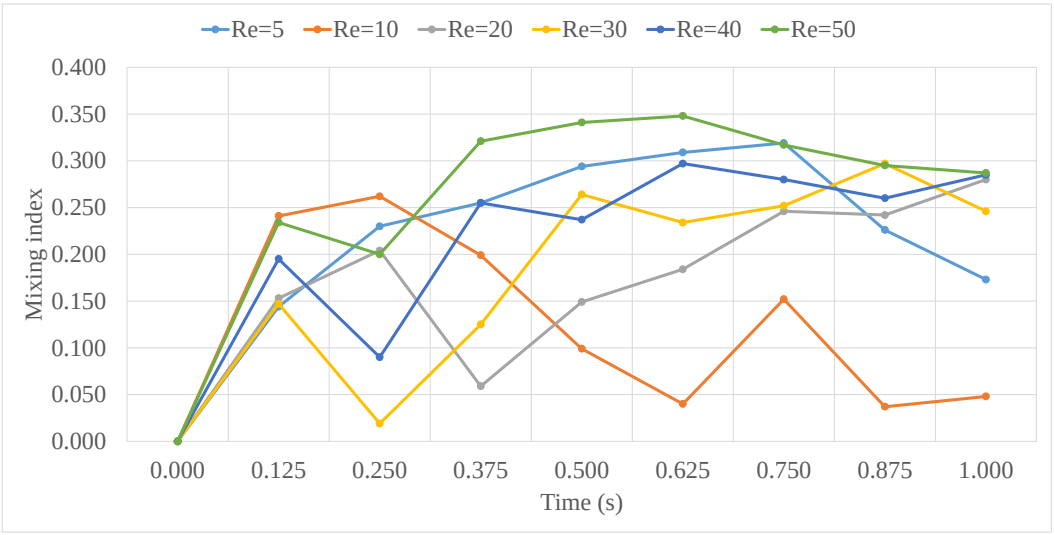

(b)

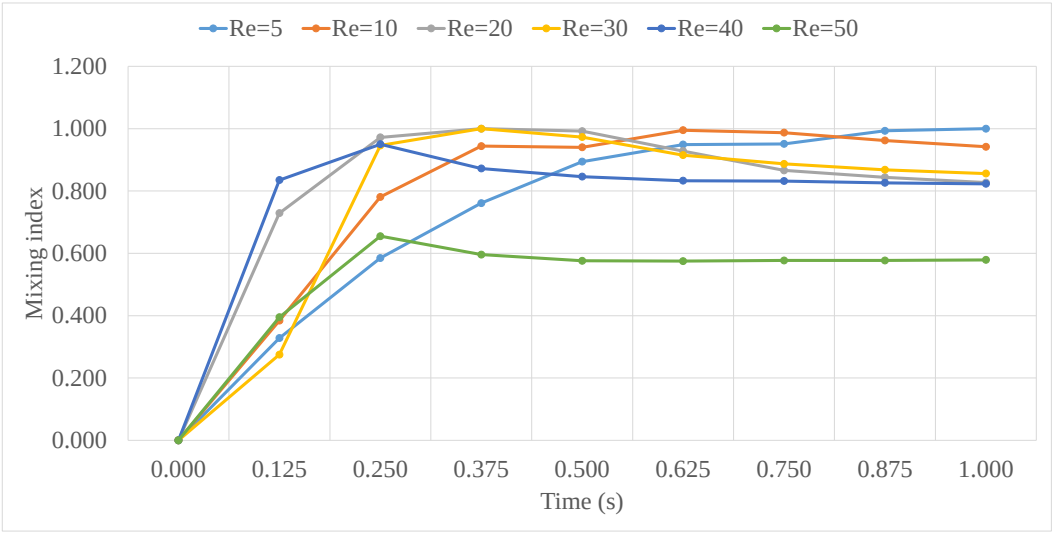

Figure 4.5: Mixing index of propan-2-ol and sodium chloride solution at (a) T-junction, and (b) offset T-junction

Figure 4.5(b) illustrates mixing index of propan-2-ol and sodium chloride solution for each Re in offset T-junction microchannel increases as time increases, but after half second, most of the value declines. This is owing to the competition between the salt ion and alcohol molecules for the water molecules (Fang et al., 2018). Since, for alcohol

molecules, fewer water molecules are available to form the hydrogen bonds; propan-2-ol remains lesser soluble in the mixture. At the end, the propan-2-ol forms a separate layer on top of the mixture (Fang et al., 2018). The two layers are easily recognizable since both have different colors as the water layer remains clearer while ‘greenish-blue’ alcohol layer is seen in this experiment as seen in Figure 4.6. It concludes that the dye inks are more soluble in the propan-2-ol. Compared to the immiscible mixing experiment performed in the T-junction microchannel earlier, this graph shows better pattern of mixing within offset T-junction microchannel.

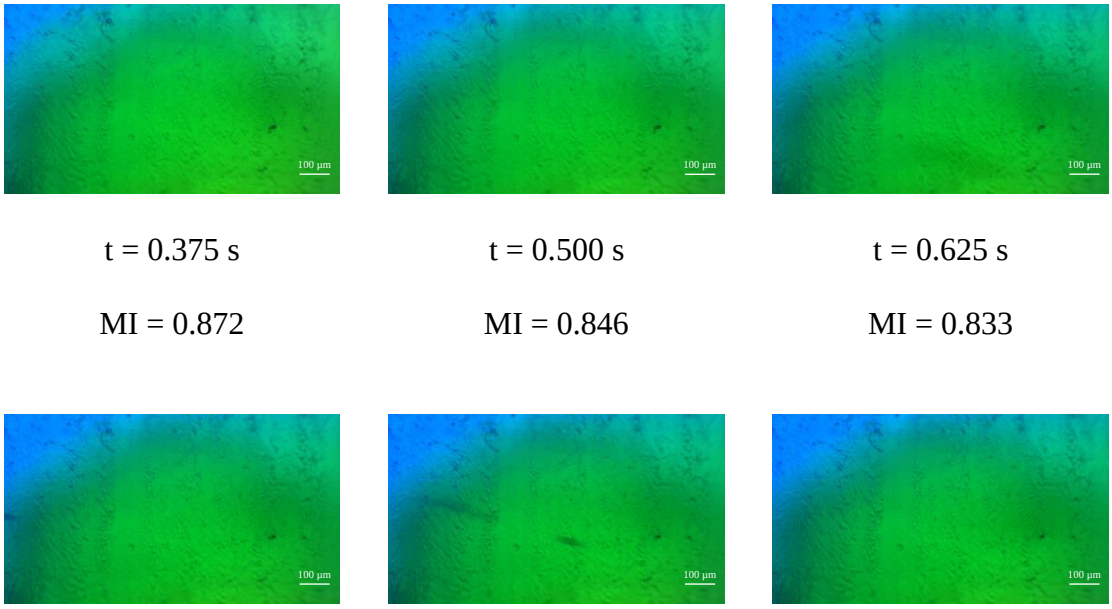

Figure 4.6: Actual mixing images (1400 µm length and 790 µm width) of blue dye in propan-2-ol and yellow dye in sodium chloride solution within offset T-junction microchannel at Re of 40. MI stands for mixing index.

The mixing behavior of two different liquids in T-junction and offset T-junction microchannels are compared. Due to dissimilar geometry, the considerable factor that may affect the initial mixing process is momentum difference between liquids at inlets (Wang et al., 2012). Based on Figure 4.7, offset T-junction microchannel offers better mixing of propan-2-ol and sodium chloride solution compared to T-junction microchannel at both low and high Re. The chaotic mixing happened within the T-junction microchannel due to the direct interaction of two liquids entering the junction at high momentum. When the inlets of T-junction having an offset of 7.5 mm, the mixing quality increases by twice or more. The inlet stream has, to some extent, the synergetic effect with molecular diffusion (Wang et al., 2012). At Re of 5, the highest mixing index at T-junction microchannel is 0.3 meanwhile offset T-junction microchannel is 1. Besides that, at high Re, the index reading at offset T-junction microchannel is twice the value of index at T-junction microchannel. However, the synergetic effect along with residence time is reduced with the increased flow rates (Wang et al., 2012). Therefore, the diffusion between two streams decreases. From the graph, mixing quality of propan-2-ol and sodium chloride solution at low Re is much better than at the Re of 50. At both high and low Re, the well-mixing behavior between propan-2-ol and sodium chloride solution is highly achieved using offset T-junction microfluidic channel.

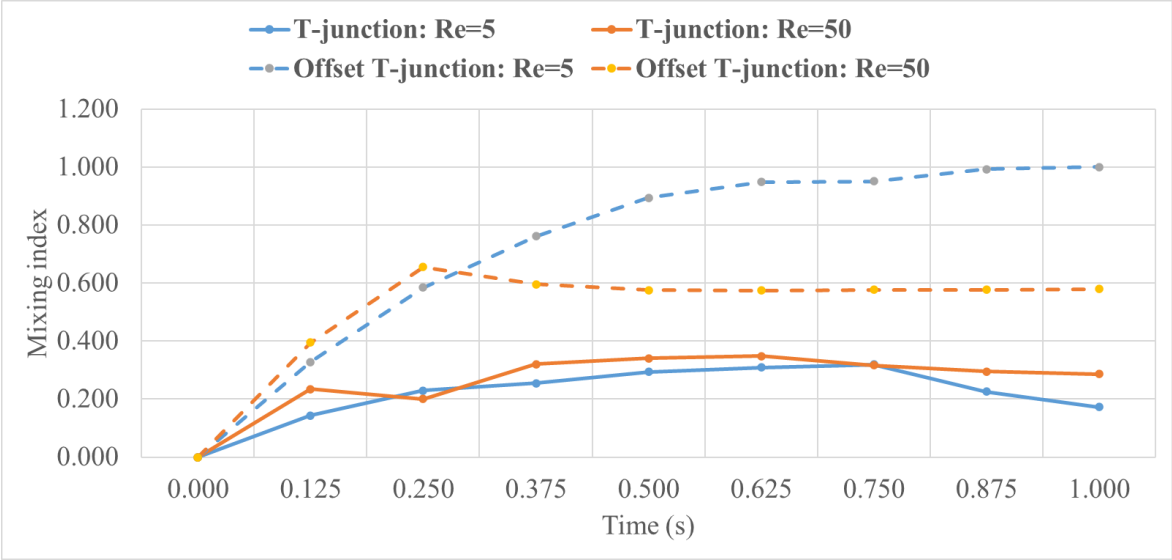

Figure 4.7: Comparison of mixing index between propan-2-ol and sodium chloride solution at different Re in T-junction and offset T-junction microchannels

4.3 Droplet Generation Results

Based on the earlier experimental results, microfluidic offset T-junction offers better performance than the T-junction channels. For this reason, the behaviours of distilled water droplet formation suspended in food grade palm olein at interfacial surface was investigated using offset T-junction microchannels having radius of 400 µm, 500 µm, 750 µm and 1000 µm via micro-PIV software.

4.3.1 Evolution of Water Droplets at The Intersection of Offset T-junction microchannel

In general, less viscous water flows faster than more viscous oil. However, when both solutions experimented in a microchannel, the hydrophobic coating on the walls of the PMMA channel (Wang et al., 2020) creates a small air gap between the inside wall of the channel and the outer surface of the liquids (Vuckovac et al., 2020). The air gap around more viscous liquid is larger, which allowed food grade palm olein to move through the channel faster than the less viscous distilled water.

Figure 4.8 shows the growth of water droplets at the junction in an offset T-microchannel at t_1 = 91 ms until t_4 = 636 ms. The droplet in microchannel with radius of 400 µm evolved faster over time compared to the droplet in channel with radius of 750 µm, and at t_4 = 636 ms, the front tip of droplet started to exceed the junction point. This growth pattern of the droplet was found similar to the ones in the channel with radius of 500 µm. However, for channel with radius of 750 µm, the evolution of the water droplet is much slower as time passed and the droplet is still within the junction area and can be seen at t_4 = 636 ms. In terms of droplet size, the droplet is bigger as the size of microchannel increases. The water droplet is rounder and more solid-shaped within microchannel's radius of 750 µm. Its size is less than or nearly equal to the microchannel's width. Both channels showed that when the droplet reached the junction, the oil pushed the water droplet upwards and cause an irregular shape at the bottom of the droplet as can be seen at t_3 = 455 ms. At this point, the droplet is likely starting to be in the break-up process. The droplet expanded mainly in radial direction and slightly in axial direction (Fu et al., 2009). Hence, the length increases gradually while the width increases moderately. This point is named as thread expansion stage and the period is called expansion time (Fu et al., 2009). As it reached $t = t_4$, the cross-flowing liquids drove the thread in its axial direction and a visible neck formed. The droplet in microchannel with radius 400 µm is faster to split and break-up compared to 750 µm channel. In short, different size of the offset T-junction microchannels induces different droplets' behaviours in term of their size and velocity, which would greatly influence the formation of neck, split and breakup process within the channel.

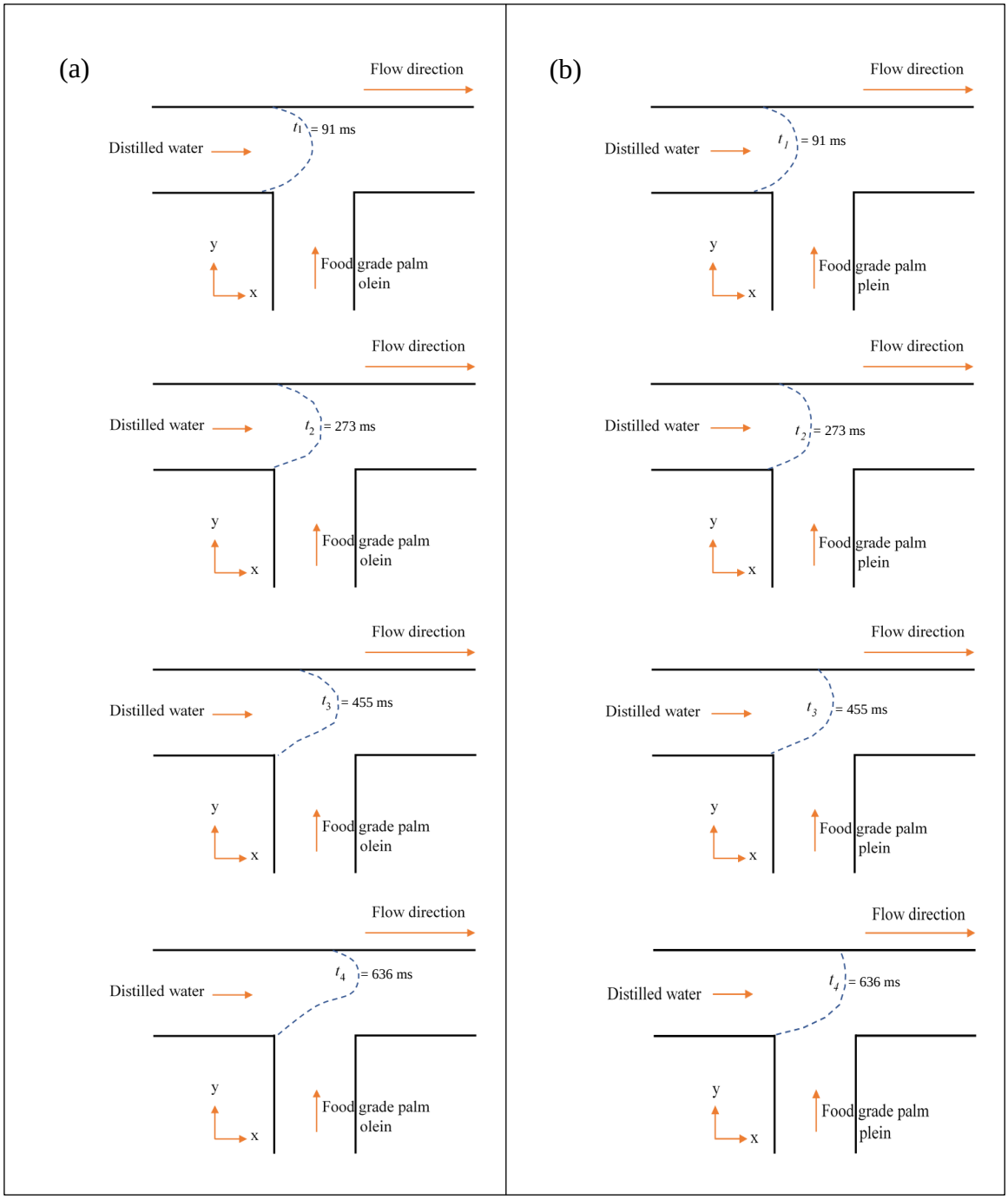

Figure 4.8: The evolution of water droplets for offset T-junction microchannels with radius of (a) 400 µm, and (b) 750 µm at t_1 = 91 ms until t_4 = 636 ms

4.3.2 Experimental Velocity of Water Droplets at The Intersection of Offset T-junction Microchannel

The experimental velocity of water droplets at the intersection of offset T-junction microchannel is determined by the gap difference between droplet at t = 91 ms and t = 455 ms. Time t = 91 ms and t = 455 ms were chosen because the front tip of the droplets for all channel still can be seen at this range of time. The front tip of the droplets is exceeded the field of view at t = 636 ms for the case of microchannel with radius 400 µm and 500 µm. Increasing in the radius of offset T-junction microchannel leads to the decrease of droplet's velocity. Velocity decreases when the cross-sectional area increases (Pang et al., 2014). This is a consequence of the continuity equation. If the flow rate is held constant, when the area decreases, the velocity must increase proportionally. Based on Table 4.1, the experimental data have proved this theory, where microchannel with radius 400 µm has higher water droplet's velocity than the channel with radius 750 µm.

The experimental velocity of the distilled water phase's also holds a good agreement with the ones that theoretical have. The surface roughness of the channel walls and the limitation of the frame rate that can be captured by the CCD camera are the several factors that might affect the liquids' flows, which cause 0.06 mm/s difference in theoretical and experimental velocity of the distilled water phase within microchannel radius of 500 µm. However, the actual roughness of the walls could not be quantified. For the inlet and outlet radius of offset T-junction microchannel = 1000 µm, the experimental velocity could not be determined due to the droplet was forming outside the field of view as the image was maintain captured at the junction.

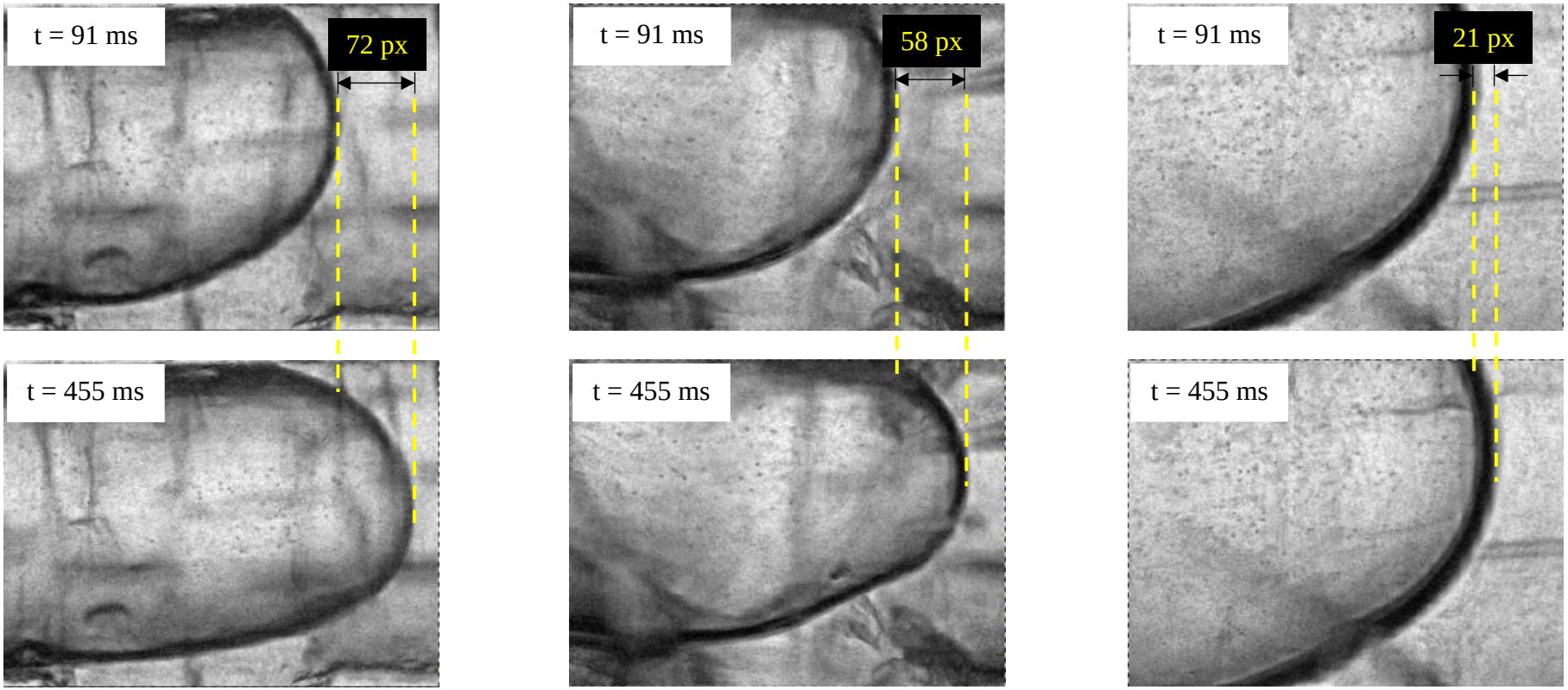

(a) (b) (c)

Figure 4.9: The motion of water droplets after 364 ms within radius of (a) 400 µm, (b) 500 µm, and (c) 750 µm offset T-junction microchannels

Table 4.1: Theoretical and experimental velocity of water droplets

Inlet and outlet radius of offset T-junction microchannel (μm)	Theoretical velocity based on Reynolds number (mm/s)	Experimental velocity of water droplets (mm/s)
400	0.322	0.330
500	0.206	0.266
750	0.092	0.096
1000	0.051	

4.3.3 Internal Velocity Profile of Generated Water Droplets in Offset T-junction Microchannel

Pre-processing images, vector analysis and also velocity magnitude analysis were performed by micro-PIV technique via MATLAB software for the droplet flow and slug flow pattern (Figure 4.10 to Figure 4.13). As the water is dispersed phase, the hydrophobic coating promotes these dispersed flows in which the water phase must wet the wall of the microchannel (Vuckovac et al., 2020).

The pattern of the flow involving droplets as shown in Figure 4.10 to Figure 4.12 can be characterized by the sub-channel sized droplets (Darekar et al., 2017). The flow within these droplets is guided forward at the interfaces to the right end of the microchannels, where the water droplets are bypassed by the continuous oil phase. The formation of such droplets, having diameter less than channel diameter, are generated at low dispersed and high continuous phase flow rates. In such conditions, the inertial force input at the higher flow rate of the continuous phase is high enough to break down the dispersed phase into smaller droplets with lesser resistance posed by the dispersed phase at lower flow rate. Meanwhile, for the slug flow pattern which is likely to be the flow

behaviour for microchannel with radius 1000 μm (Figure 4.13), the slug occupied almost the whole cross-section of the microchannel with a very thin layer of the oil phase between the slug and the wall of the offset T-junction microchannel and this behaviour fit well in Darekar et al. (2017) flow regime map. It is evident from this discussion that changing the channel size has a significant impact on the slug size. In contrast to smaller offset T-junction microchannel, bigger channel produce larger slugs. All of the microchannels exhibit same slug size behaviours in relation to flow velocity (Kashid & Agar, 2007). However, the shear stress is not significant in this regime and the interfacial tension along with the pressure gradient results in the breakup of dispersed phase into slug. The interfacial tension could not support and endure the pressure gap between inside and outside the interface at the droplet's tail (Liu et al., 2017). This pressure differential increases prior to the neck regime, squeezing the interface, and consequently forced the rear tip or interface to break, resulting in the formation of a droplet. Resultantly, the slug growth leads to the obstruction to the continuous phase flow (Darekar et al., 2017).

In terms of the microchannel's size affecting the size of droplet, based on Figure 4.10 to Figure 4.12, the droplets' size increases with an increase in the radius of the microchannels. In the case of small differences between the offset T-junction microchannels i.e., radius of 400 μm and 500 μm, there is no major difference in droplets' sizes can be spotted from Figure 4.10 and Figure 4.11. However, with further increase in the microchannel's radius to 750 μm (Figure 4.12), the water droplet size with respect to flow velocity increases significantly. For the microchannel with radius of 1000 μm (Figure 4.13), the droplet's volume cannot be seen due to the limit of field of view and the exceedance of the observation area. From this discussion, it is clear that the change in the offset T-junction microchannel's radius exerts a major influence on the water droplet size.

On the other hand, the flow velocity vectors determined by micro-PIV are displayed as small arrows. The key features of the flow are illustrated by larger arrows for better visualization. At t = 91 ms and t = 1000 ms, microchannel with radius of 750 μm (Figure 4.12) has average velocity of 0.055 mm/s and 0.15 mm/s which is 2.7 and 1.3 times smaller than the average velocity of microchannel with radius of 500 μm (Figure 4.11), respectively. This is because in a bigger channel, the oil phase is eventually taking longer time to break down the water phase into longer slugs. The interfacial area was decreased as channel size was increased. In contrast to that, for a smaller channel, an increase in the velocity with respect to time increases its inertial force which leads to the enhancement in its tendency to break down the water phase into smaller droplets form. In short, increasing the channel's diameter and cross-sectional area decrease the liquid's velocity compared to the ones in the smaller channel. This also can be proved by referring to the Hagen-Poiseuille equation (Liu & Pang, 2015) below:

$$Q_{HP} = \frac{\pi R^4 \Delta p}{8\mu L} \qquad \text{Equation 4.1}$$

where Q_{HP} is flow rate, R is the channel's radius, Δp is the pressure drop between the inlet and outlet, μ is the dynamic viscosity of the fluid, and L is the channel's length.

The velocity could then be shown as,

$$v_{HP} = \frac{Q_{HP}}{A} = \frac{R^2 \Delta p}{8\mu L} \qquad \text{Equation 4.2}$$

where v_{HP} is the average velocity, A is the channel's cross-sectional area.

Let Q_{exp} to be the flow rate measured in the experiment, the velocity can thus be written as,

$$v_{exp} = \frac{Q_{exp}}{A}$$ Equation 4.3

The highest velocity which coloured in yellow region in velocity magnitude analysis is highly due to the vortex which localised near towards the edge of the droplet, as the droplet growing bigger and the particles also moved to the edge. The interfacial tension between the droplet and the continuous oil phase pulls the resulting interface sideways more firmly, causing powerful vortex motions within the water droplet. The shear force causes this strong vortex motions within the droplet, located away from center to the edge of the front inner surface, deflecting the accelerated dispersed water phase (Jin & Yoo, 2012). Since gravitational forces have no significant impact in microfluidics, it can be concluded that the central region of the inner droplets exhibits low velocities, while the regions near the channel boundaries have higher velocities magnitude (Ma et al., 2015). This can be shown in Figure 4.10 (iii), Figure 4.11 (iii) and Figure 4.12 (iii) where t = 455 ms. There might be minimal errors in the readings due to the channel's inner geometry and its surface roughness during the fabrication process. In addition, the maximum frame rate that can be captured is limited by the installed CCD camera used in the microscope.

(a) radius of 400 µm offset T-microchannel

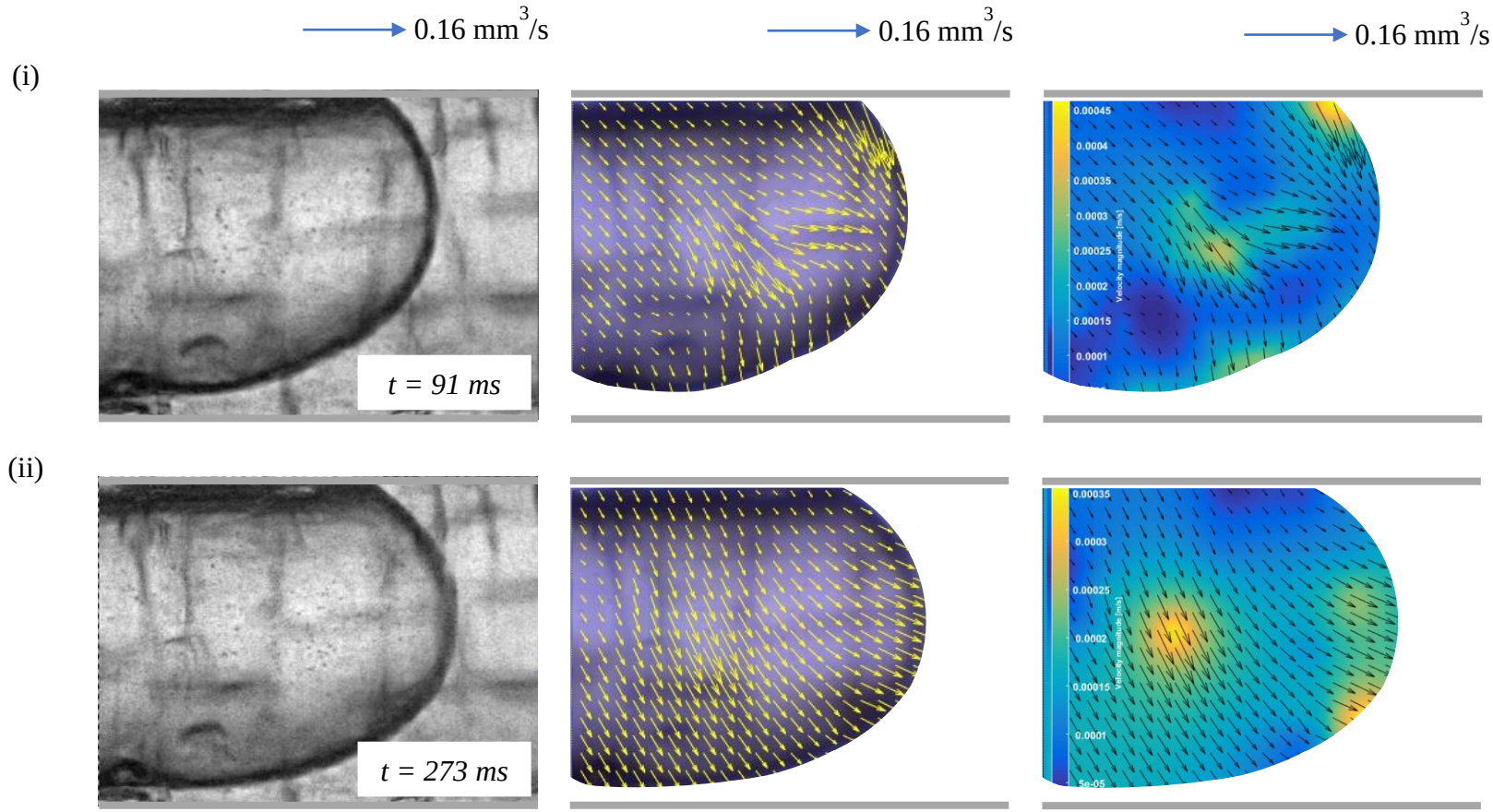

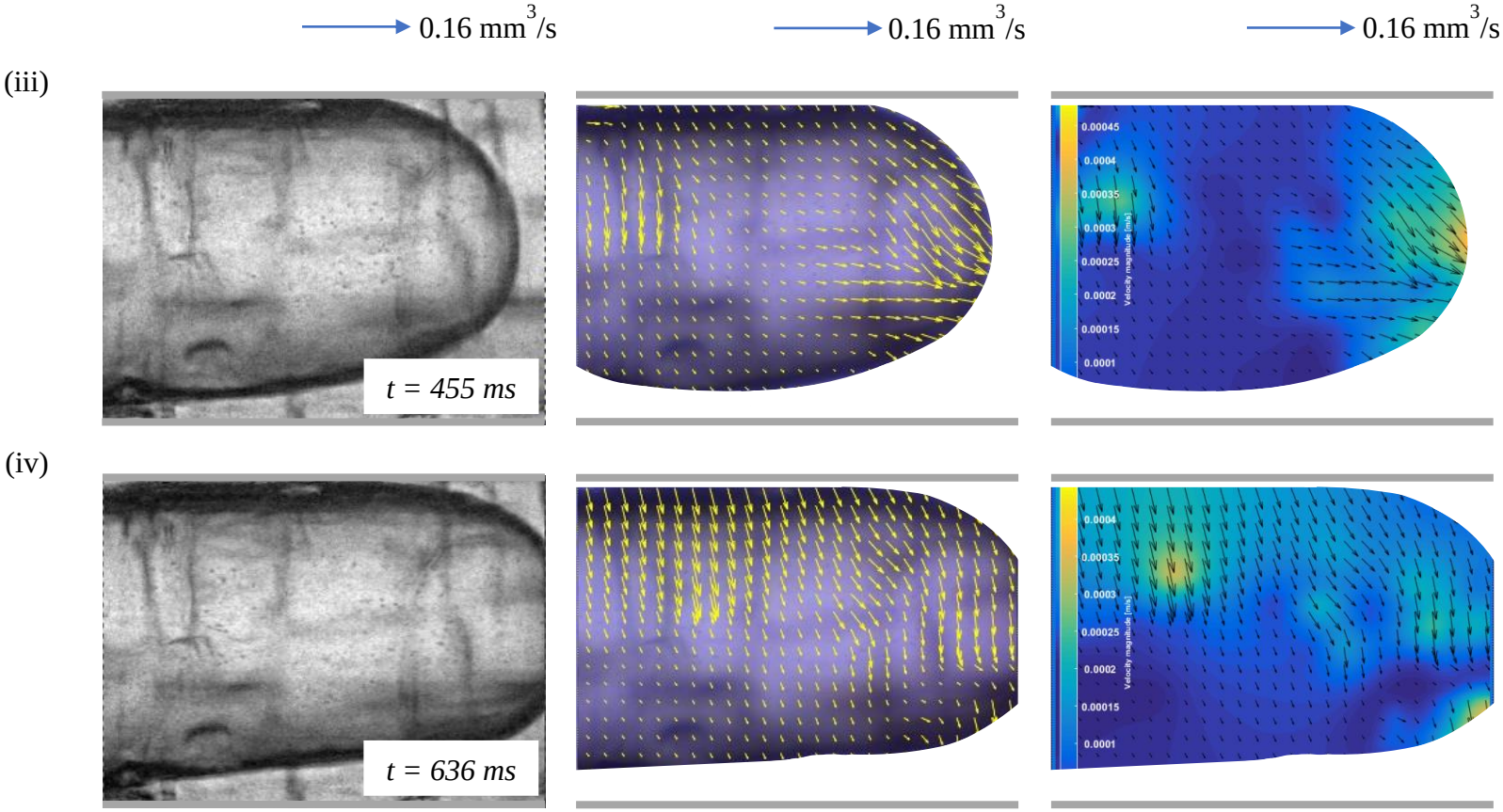
0.16 mm3/s
0.16 mm3/s
0.16 mm3/s
(iii)
t = 455 ms
(iv)
t = 636 ms
0.00045
0.0004
0.00035
0.0003
0.00025
0.0002
0.00015
0.0001
Velocity magnitude [m/s]

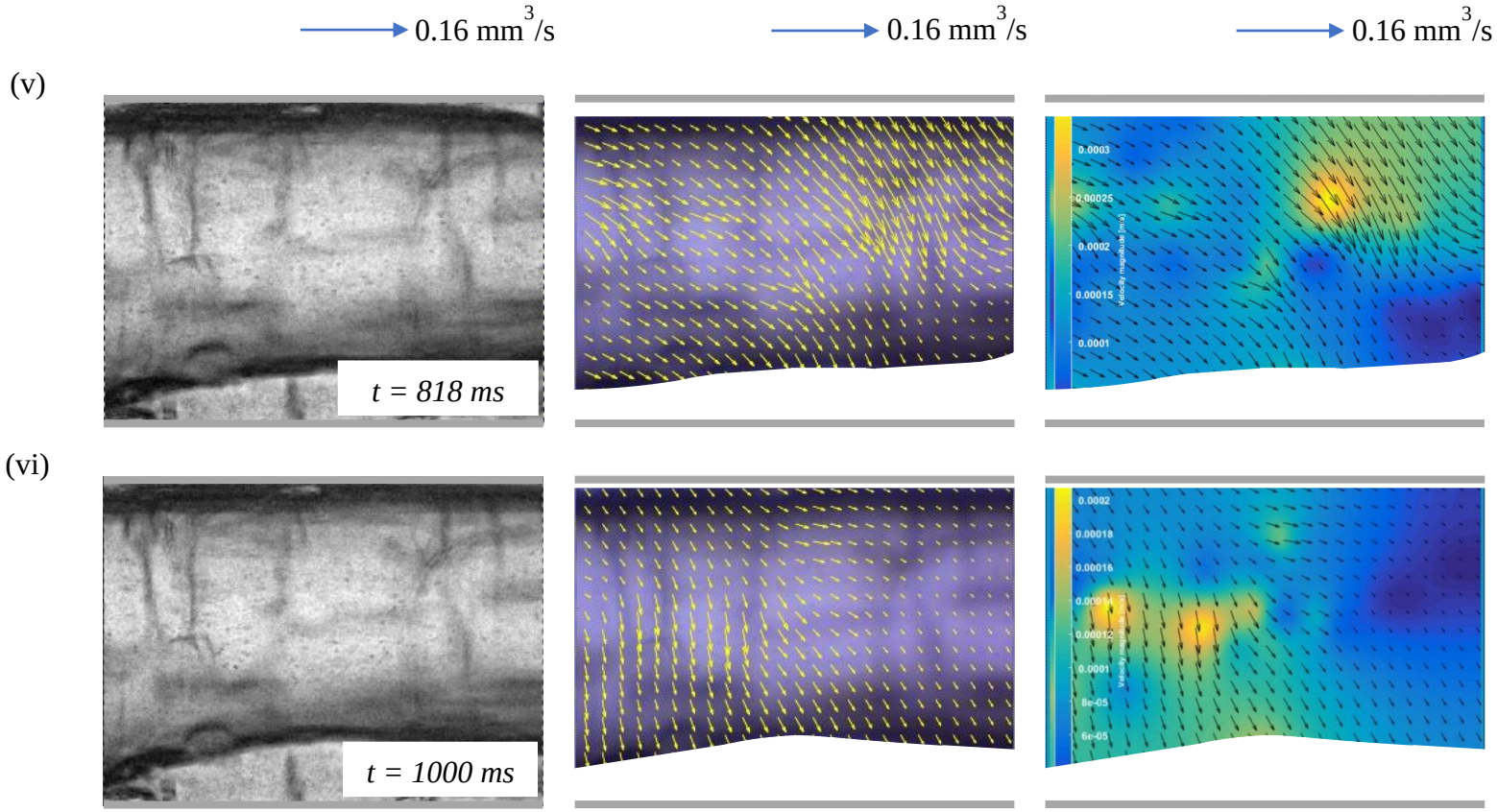

Figure 4.10: Internal velocity profile of generated water droplet for offset T-junction microchannel with radius of 400 µm

(b) radius of 500 µm offset T-microchannel

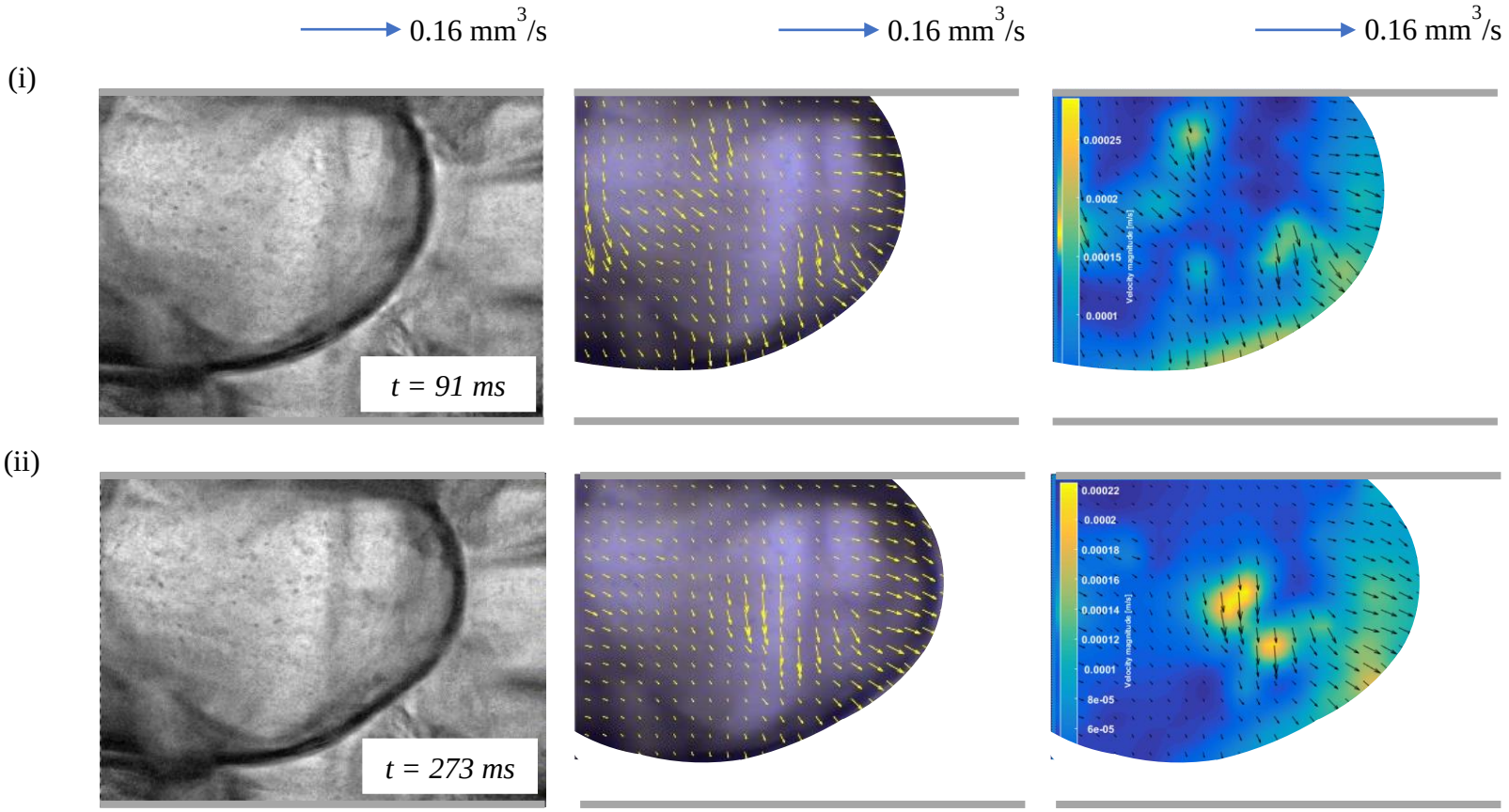

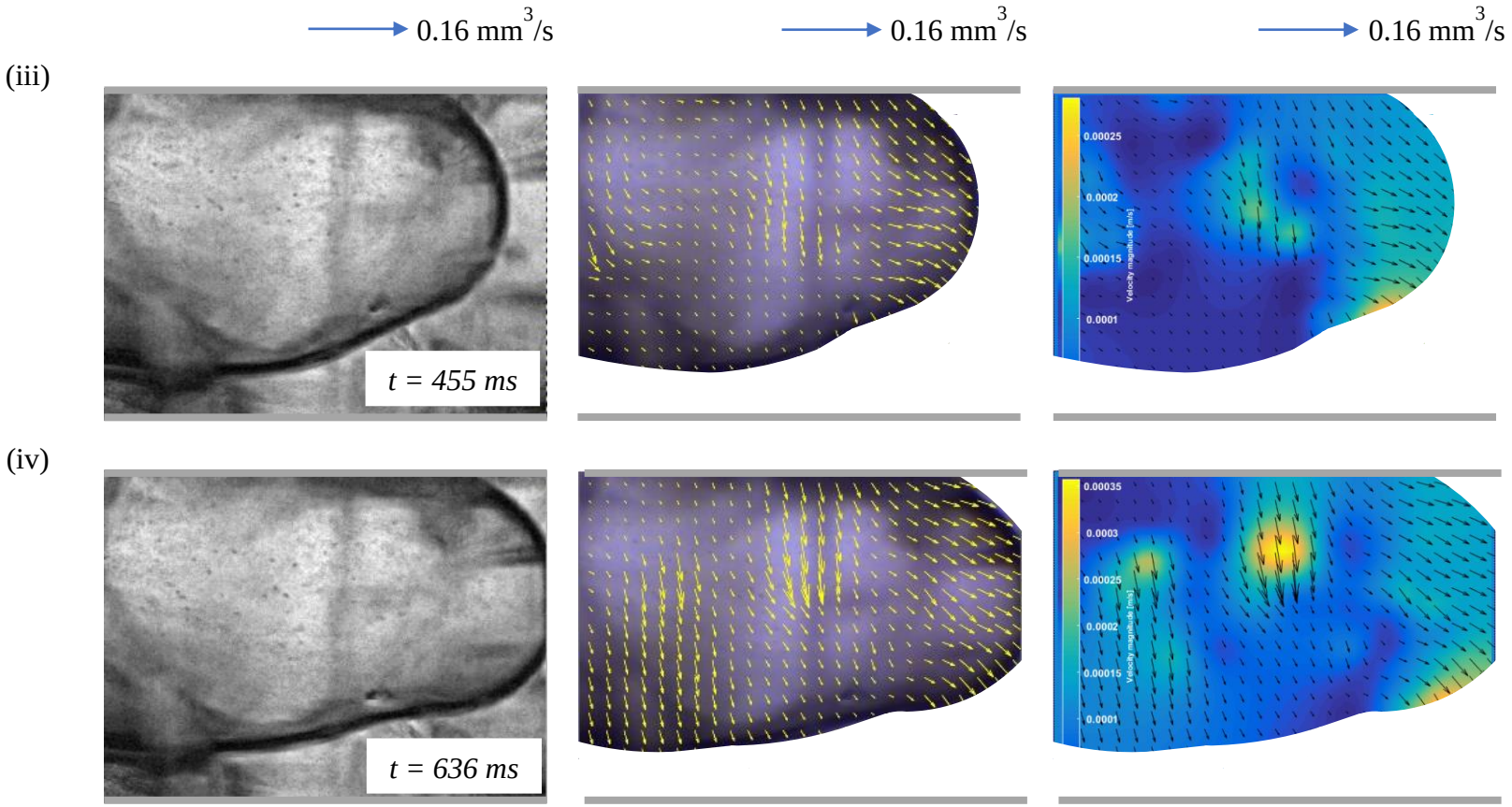
0.16 mm3/s
0.16 mm3/s
0.16 mm3/s
(iii)
t = 455 ms
0.00025
0.0002
0.00015
0.0001
Velocity magnitude [m/s]
(iv)
t = 636 ms
0.00035
0.0003
0.00025
0.0002
0.00015
0.0001

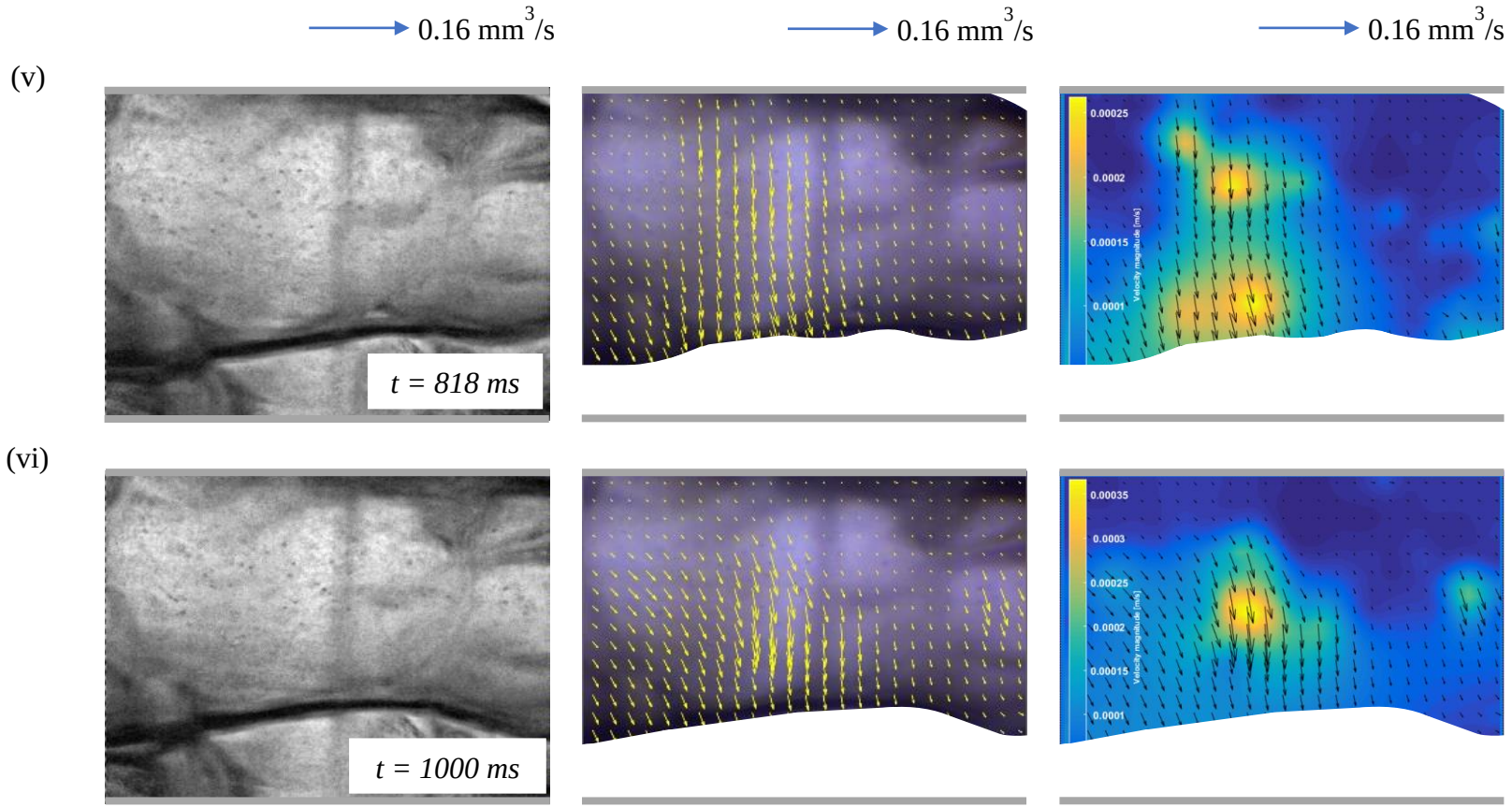

Figure 4.11: Internal velocity profile of generated water droplet for offset T-junction microchannel with radius of 500 µm

(c) radius of 750 µm offset T-microchannel

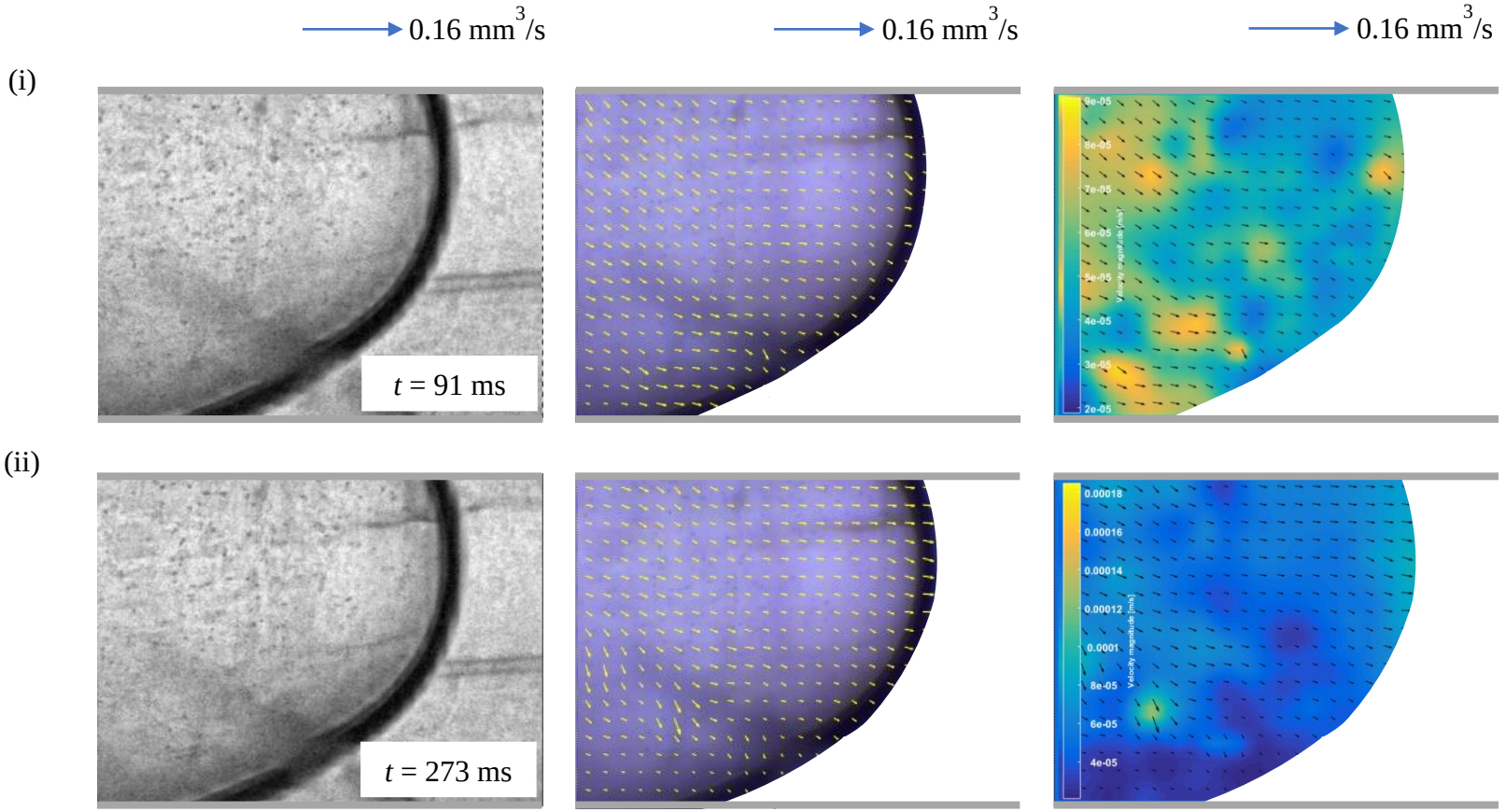

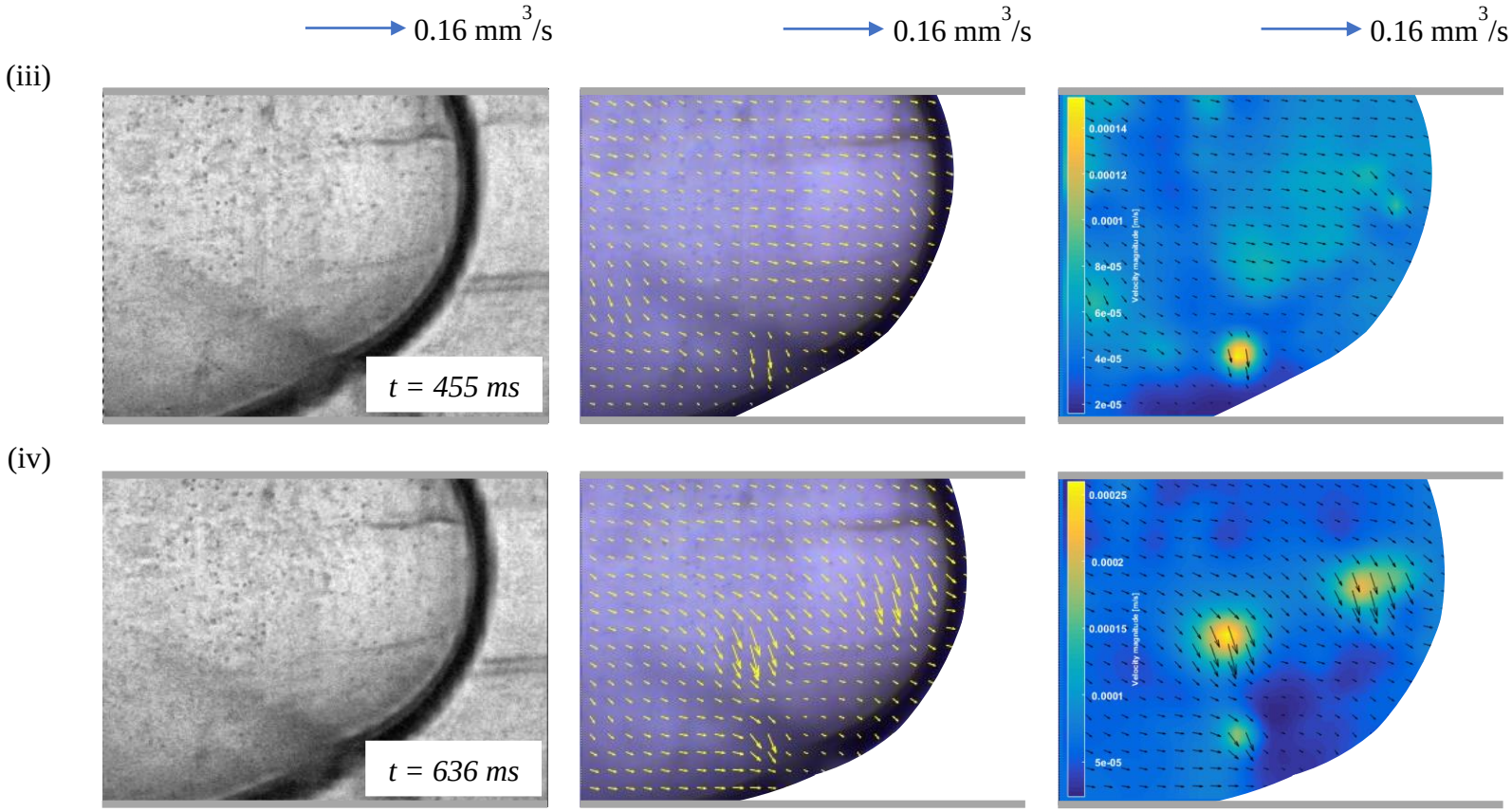
0.16 mm3/s
0.16 mm3/s
0.16 mm3/s
(iii)
t = 455 ms
0.00014
0.00012
0.0001
8e-05
6e-05
4e-05
2e-05
(iv)
t = 636 ms
0.00025
0.0002
0.00015
0.0001
5e-05

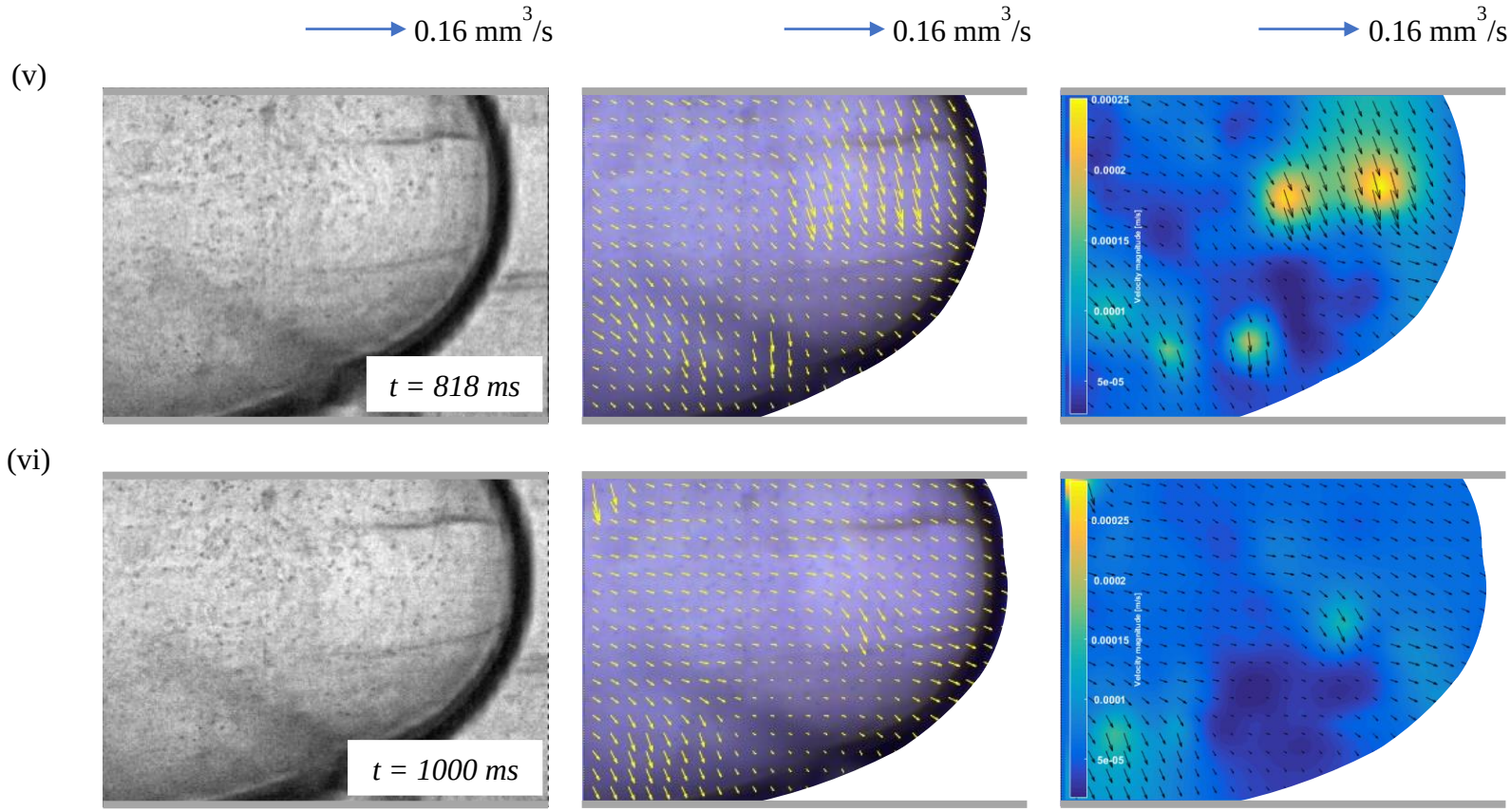

Figure 4.12: Internal velocity profile of generated water droplet for offset T-junction microchannel with radius of 750 µm

(d) radius of 1000 µm offset T-microchannel

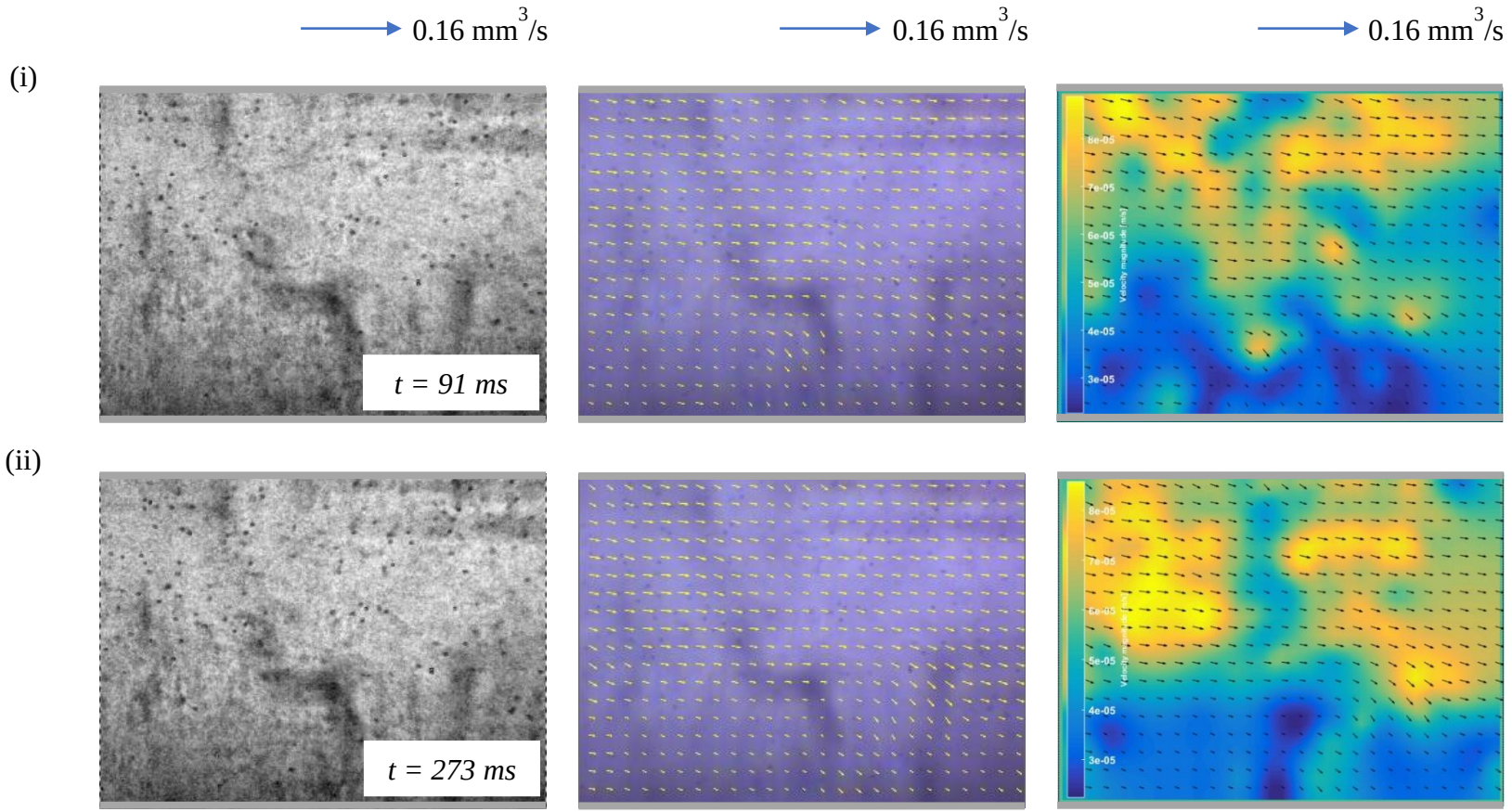

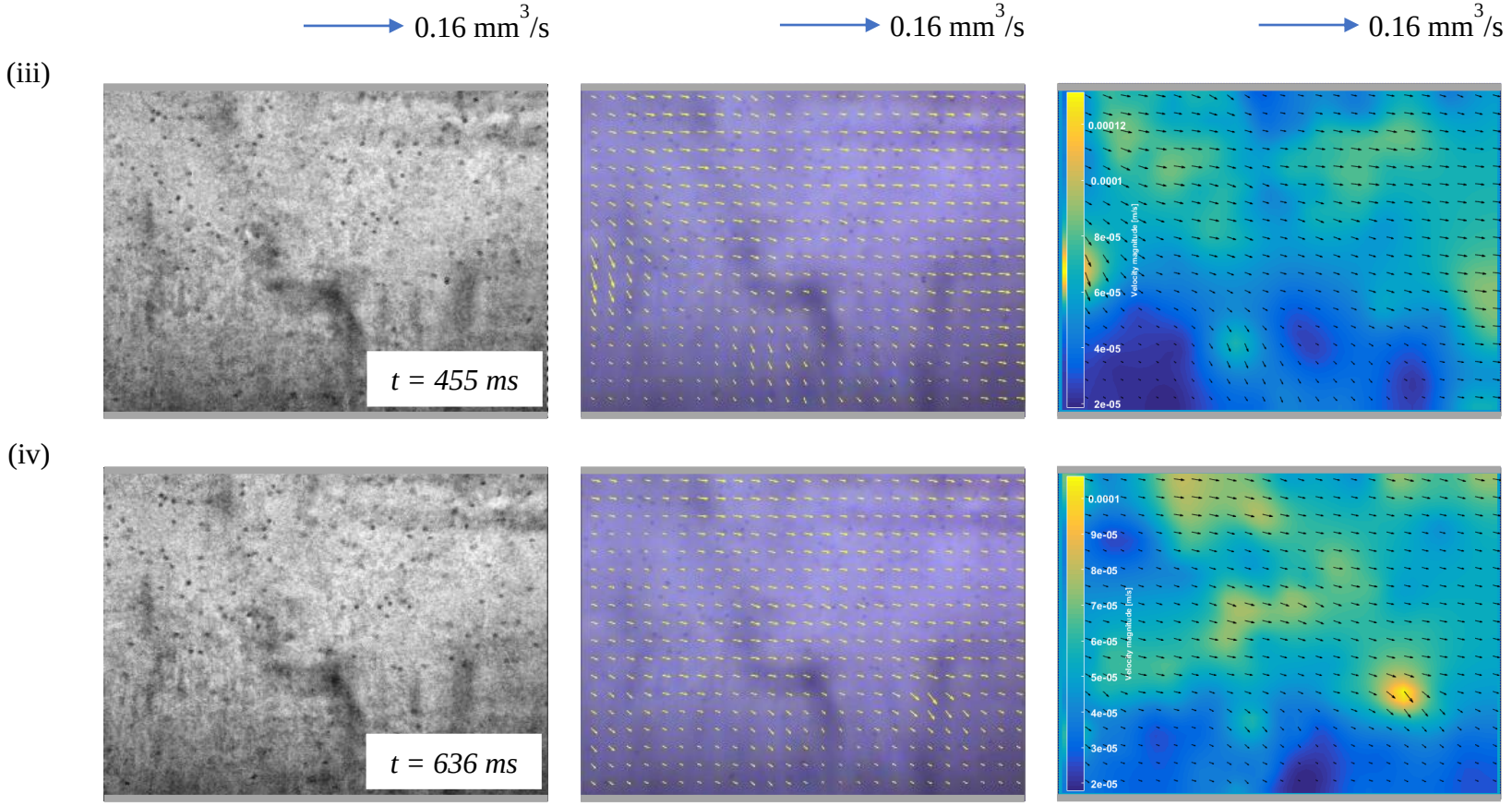
0.16 mm3/s
0.16 mm3/s
0.16 mm3/s
(iii)
t = 455 ms
0.00012
0.0001
8e-05
6e-05
4e-05
2e-05
Velocity magnitude [m/s]
(iv)
t = 636 ms
0.0001
9e-05
8e-05
7e-05
6e-05
5e-05
4e-05
3e-05
2e-05
Velocity magnitude [m/s]

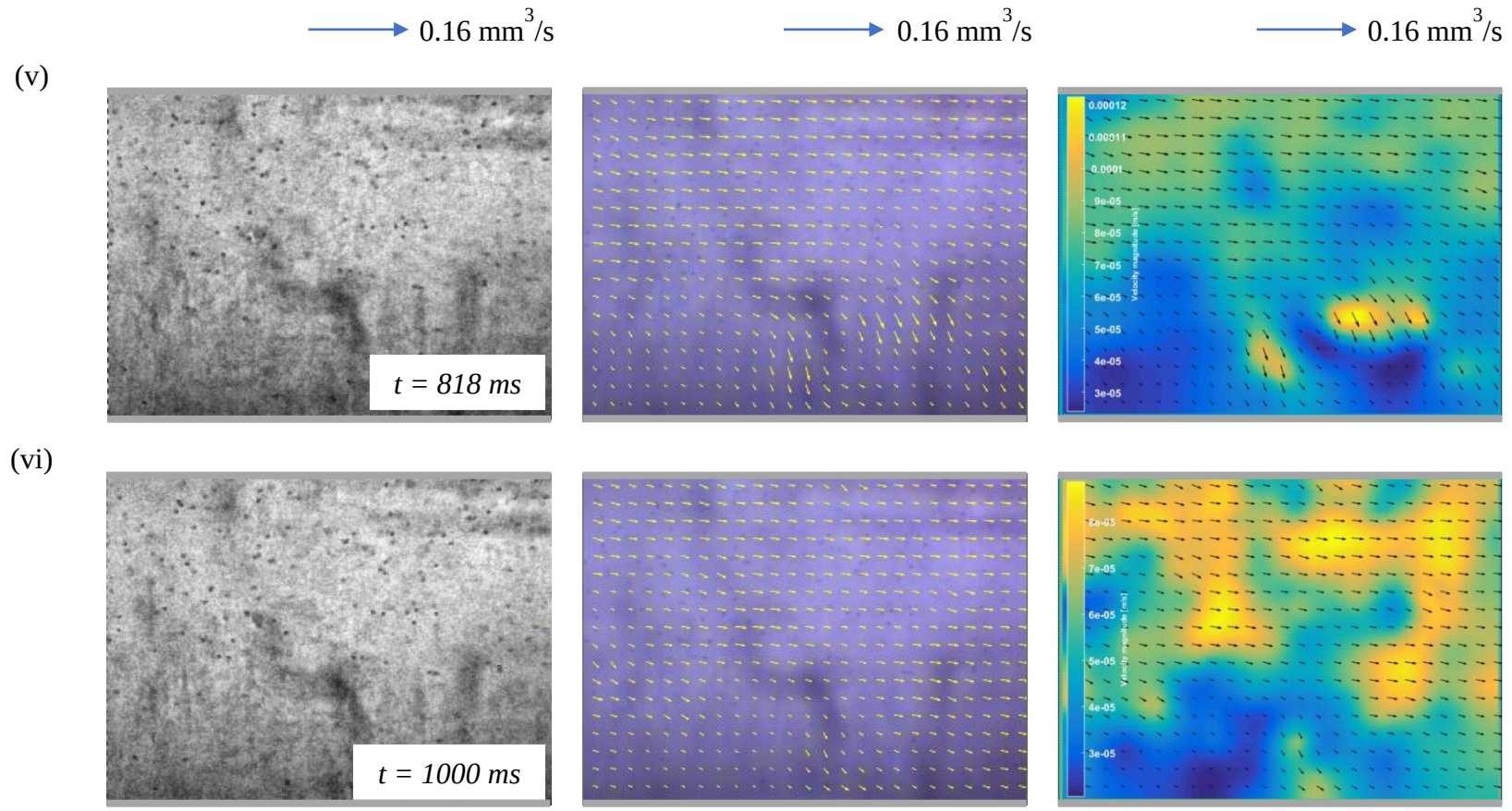

Figure 4.13: Internal velocity profile of generated water droplet for offset T-junction microchannel with radius of 1000 µm

4.4 Summary

As a summary, both microchannels for miscible mixing experiments show better performance as mixing time for each Re increases, especially at high Reynolds number (Re) of 40 and 50 while for immiscible mixture, the mixing index fluctuates in the range of $5 \leq Re \leq 50$. Between T-junction and offset T-junction microchannel, the latter yielded superior mixing performance than the former at both low and high Re of immiscible mixing. Therefore, the droplet generation study at interfacial surface was investigated using offset T-junction microchannels having radius of 400 µm, 500 µm, 750 µm and 1000 µm via micro-PIV software. The results showed that experimental velocity of the water droplet holds good agreement with theoretical values, having minimal difference as low as 0.004 mm/s for the case of microchannel with radius 750 µm. In addition, a major elevation for mean velocity from 0.055 mm/s to 0.15 mm/s was also seen in this channel. The vector and velocity magnitude data also in a good agreement with Hagen-Poiseuille flow equation, which states that channel with bigger diameter resulting in an increase in overall flow of a liquid.

CHAPTER 5

CONCLUSION AND RECOMMENDATIONS

5.1 Conclusion

In this study, two different designs of microchannels i.e., T-junction and offset T-junction were successfully designed and fabricated to characterize mixing index of dissimilar liquids i.e., propan-2-ol, water and sodium chloride solution at $5 \leq Re \leq 50$. For miscible mixing experiments i.e., propan-2-ol and water, water and sodium chloride solution, both microchannels show that mixing performance of these liquids is directly proportional to the mixing time for each Re. This is because at low Re of 5, 10 and 20, the higher residence time allows for higher molecular diffusion as the flow rate is low. Besides that, viscosity-density difference also contributed to the increased of mixing index as high viscous and more dense liquid pushed a low viscous and less dense liquid from the channel wall which resulted in an increase of the interface area and consequently improved the mixing in this regime. On the other hand, it is nearly impossible to mix propan-2-ol and sodium chloride solution in the microchannel. In fact, molecular diffusion process between these immiscible liquids is difficult compared to the previous two miscible mixing experiments. Nevertheless, offset T-junction microchannel offers better mixing of propan-2-ol and sodium chloride solution compared to T-junction microchannel at both low and high Re. Due to the direct collision at the T-junction of the microchannel, chaotic mixing takes place at the intersection at high momentum. When the inlets of T-junction having an offset of 7.5 mm, the mixing quality increases by twice or more.

Due to the fact that offset T-junction can give superior performance than T-junction for immiscible mixture, this work was furthered by studying the behaviours of distilled

water droplet formation suspended in food grade palm olein at interfacial surface in offset T-microchannel having radius of 400 µm, 500 µm, 750 µm and 1000 µm by means of micro-PIV software. These different sizes of inlet and outlet radius of microfluidic channels were affecting the flow behaviours of the multiphase liquids, and also generation of the water droplets i.e., formation of neck, split and break-up process. The experimental results show that increasing in the radius of offset T-junction microchannel leads to the increase in cross-sectional area and the decrease of distilled water phase's velocity. Besides that, the experimental velocity of the distilled water phase's holds a good agreement with theoretical values The size of the droplets is getting bigger and nearly equal to the microchannel's width as the radius of microchannel increases. At t = 1000 ms, the average velocity of channel with radius of 400 µm decreased slightly to 0.12 mm/s which might due to the roughness on the channel's surface, while the other channels showed a good and maintained average velocity data. This concludes that the vector and velocity magnitude data in a good agreement with Hagen-Poiseuille flow equation, meaning that a small increase in the channel's internal diameter yields a significant increase in overall flow of a liquid.

5.2 Recommendations

The characterization of mixing index and the droplet generation requires some improvement, especially in terms of the microscope's working principle/ability as it is believably influencing the overall performance of the system. The recommendations are as follow:

(a) Higher power objective lens i.e., 20× magnification as it can provide a higher degree of magnification, which allows to zoom in closer to the sample being studied and see it in more detail.

(b) Higher frame rate, so that smoother and slower the slow motion of fluid flow as the number of frames captured per second increase while maintaining its resolution to produce even more higher quality images.

(c) The design of offset T-junction microchannel can be used to study mixing performance of two-phase separation immiscible liquids, for example in biology analysis. This is because the offset T-junction microchannel could offer better performance than conventional T-junction microchannel.

(d) A relative study investigating the effect of channel wall i.e., PMMA, silicone elastomer (PDMS) and glass on mixing performance and droplet generation behaviours is proposed. This is due to the influence of their surface roughness and hydrophobicity or hydrophilicity characteristics to the liquid's behaviours.

(e) To investigate the effects of swapping the position of liquid inlets on the microfluidic mixing performance of two dissimilar liquids.

REFERENCES

Ansari, M., Kim, K.-Y., & Kim, S. M. (2010). Numerical study of the effect on mixing of the position of fluid stream interfaces in a rectangular microchannel. *Microsystem technologies, 16*(10), 1757-1763.

Ansari, M. A., Kim, K.-Y., & Kim, S. M. (2018). Numerical and experimental study on mixing performances of simple and vortex micro T-mixers. *Micromachines, 9*(5), 204.

Aubin, J., Ferrando, M., & Jiricny, V. (2010). Current methods for characterising mixing and flow in microchannels. *Chemical Engineering Science, 65*(6), 2065-2093.

Campo-Deaño, L. (2018). Fluid-flow characterization in microfluidics. *Complex Fluid-Flows in Microfluidics* (pp. 53-71): Springer.

Chen, C.-H., Shah, R. K., Abate, A. R., & Weitz, D. A. (2009). Janus particles templated from double emulsion droplets generated using microfluidics. *Langmuir, 25*(8), 4320-4323.

Chen, X., Li, T., Zeng, H., Hu, Z., & Fu, B. (2016). Numerical and experimental investigation on micromixers with serpentine microchannels. *International Journal of Heat and Mass Transfer, 98,* 131-140.

Chung, C.-K., & Shih, T. (2008). Effect of geometry on fluid mixing of the rhombic micromixers. *Microfluidics and Nanofluidics, 4*(5), 419-425.

Colucci, G., Santamaria-Echart, A., Silva, S. C., Fernandes, I. P., Sipoli, C. C., & Barreiro, M. F. (2020). Development of Water-in-Oil Emulsions as Delivery Vehicles and Testing with a Natural Antimicrobial Extract. *Molecules, 25*(9), 2105.

Dambrine, J., Geraud, B., & Salmon, J. (2009). Interdiffusion of liquids of different viscosities in a microchannel. *New Journal of Physics, 11*(7), 075015.

Darekar, M., Singh, K. K., Mukhopadhyay, S., & Shenoy, K. T. (2017). Liquid–liquid two-phase flow patterns in Y-junction microchannels. *Industrial & Engineering Chemistry Research, 56*(42), 12215-12226.

Deng, C., Huang, W., Wang, H., Cheng, S., He, X., & Xu, B. (2018). Preparation of Micron-Sized Droplets and Their Hydrodynamic Behavior in Quiescent Water. *Brazilian Journal of Chemical Engineering, 35*(2), 709-720.

Dreher, S., Kockmann, N., & Woias, P. (2009). Characterization of laminar transient flow regimes and mixing in T-shaped micromixers. *Heat Transfer Engineering, 30*(1-2), 91-100.

Dundi, M., VRK, R., & VP, C. (2019). Characterization of enhanced liquid mixing in T-T mixer at various Reynolds numbers. *Asia-Pacific Journal of Chemical Engineering, 14*(2), e2298.

Fang, C., Wu, H., Lee, S.-Y., Mahajan, R. L., & Qiao, R. (2018). The ionized graphene oxide membranes for water-ethanol separation. *Carbon, 136*, 262-269.

Fornerod, M. J., Amstad, E., & Guldin, S. (2020). Microfluidics of binary liquid mixtures with temperature-dependent miscibility. *Molecular Systems Design & Engineering*.

Fournier, M.-C., Falk, L., & Villermaux, J. (1996). A new parallel competing reaction system for assessing micromixing efficiency—experimental approach. *Chemical Engineering Science, 51*(22), 5053-5064.

Fu, H., Liu, X., & Li, S. (2017). Mixing indexes considering the combination of mean and dispersion information from intensity images for the performance estimation of micromixing. *RSC Advances, 7*(18), 10906-10914.

Fu, T., Ma, Y., Funfschilling, D., & Li, H. Z. (2009). Bubble formation and breakup mechanism in a microfluidic flow-focusing device. *Chemical Engineering Science, 64*(10), 2392-2400.

Gelin, P., Bihi, I., Ziemecka, I., Thienpont, B., Christiaens, J., Hellemans, K., . . . De Malsche, W. (2020). Microfluidic device for high-throughput production of monodisperse droplets. *Industrial & Engineering Chemistry Research, 59*(28), 12784-12791.

Giasuddin, H. M., Sanjayan, J. G., & Ranjith, P. (2013). Strength of geopolymer cured in saline water in ambient conditions. *Fuel, 107*, 34-39.

Günther, A., Jhunjhunwala, M., Thalmann, M., Schmidt, M. A., & Jensen, K. F. (2005). Micromixing of miscible liquids in segmented gas− liquid flow. *Langmuir, 21*(4), 1547-1555.

Hagsäter, S. M., Jensen, T. G., Bruus, H., & Kutter, J. P. (2007). Acoustic resonances in microfluidic chips: full-image micro-PIV experiments and numerical simulations. *Lab on a Chip, 7*(10), 1336-1344.

Hein, M., Moskopp, M., & Seemann, R. (2015). Flow field induced particle accumulation inside droplets in rectangular channels. *Lab on a Chip, 15*(13), 2879-2886.

Heydari, R., & Mousavi, M. (2016). Simultaneous determination of saccharine, caffeine, salicylic acid and benzoic acid in different matrixes by salt and air-assisted homogeneous liquid-liquid extraction and high-performance liquid chromatography. *Journal of the Chilean Chemical Society, 61*(3), 3090-3094.

Idris, C. A. C., Sundram, K., & Razis, A. F. A. (2018). Effect of Consumption Heated Oils with or without Dietary Cholesterol on the Development of Atherosclerosis. *Nutrients, 10*(10), 1527.

Jakiela, S., Korczyk, P. M., Makulska, S., Cybulski, O., & Garstecki, P. (2012). Discontinuous transition in a laminar fluid flow: a change of flow topology inside a droplet moving in a micron-size channel. *Physical Review Letters, 108*(13), 134501.

Jeon, M. K., Kim, J.-H., Noh, J., Kim, S. H., Park, H. G., & Woo, S. I. (2004). Design and characterization of a passive recycle micromixer. *Journal of Micromechanics and Microengineering, 15*(2), 346.

Jin, B.-J., & Yoo, J. Y. (2012). Visualization of droplet merging in microchannels using micro-PIV. *Experiments in Fluids, 52*(1), 235-245.

Joensson, H. N., & Andersson, H. S. (2012). Droplet microfluidics—A tool for single-cell analysis. *Angewandte Chemie International Edition, 51*(49), 12176-12192.

Kashid, M. N., & Agar, D. W. (2007). Hydrodynamics of liquid–liquid slug flow capillary microreactor: flow regimes, slug size and pressure drop. *Chemical Engineering Journal, 131*(1-3), 1-13.

Kim, C.-K., & Yoon, J.-Y. (2017). Optimal design of groove shape on passive micromixer using design of experiment technique. *Proceedings of the Institution of Mechanical Engineers, Part E: Journal of Process Mechanical Engineering, 231*(4), 880-887.

Kim, M. J., & Breuer, K. S. (2007). Use of bacterial carpets to enhance mixing in microfluidic systems. *Journal of Fluids Engineering, 129*(3), 319-324.

Kinoshita, H., Kaneda, S., Fujii, T., & Oshima, M. (2007). Three-dimensional measurement and visualization of internal flow of a moving droplet using confocal micro-PIV. *Lab on a Chip, 7*(3), 338-346.

Kumar Mondal, P., & Wongwises, S. (2020). Magneto-hydrodynamic (MHD) micropump of nanofluids in a rotating microchannel under electrical double-layer effect.

Proceedings of the Institution of Mechanical Engineers, Part E: Journal of Process Mechanical Engineering, 234(4), 318-330.

Kuntaegowdanahalli, S. S., Bhagat, A. A. S., Kumar, G., & Papautsky, I. (2009). Inertial microfluidics for continuous particle separation in spiral microchannels. *Lab on a Chip, 9*(20), 2973-2980.

Lee, C.-Y., Chang, C.-L., Wang, Y.-N., & Fu, L.-M. (2011). Microfluidic mixing: a review. *International Journal of Molecular Sciences, 12*(5), 3263-3287.

Lee, C.-Y., & Fu, L.-M. (2018). Recent advances and applications of micromixers. *Sensors and Actuators B: Chemical, 259*, 677-702.

Li, C., Boban, M., & Tuteja, A. (2017). Open-channel, water-in-oil emulsification in paper-based microfluidic devices. *Lab on a Chip, 17*(8), 1436-1441.

Li, H., Liu, H., Fang, J., Yin, S., Chen, C., & Li, C. (2019). Isopropanol, n-butanol and ethanol recovery from IBE model solutions by salting-out using potassium pyrophosphate. *Journal of Chemical Technology and Biotechnology*, *94*(12), 3850-3858.

Lin, Y.-C., Chung, Y.-C., & Wu, C.-Y. (2007). Mixing enhancement of the passive microfluidic mixer with J-shaped baffles in the tee channel. *Biomedical Microdevices, 9*(2), 215-221.

Lin, Y., Yu, X., Wang, Z., Tu, S.-T., & Wang, Z. (2011). Design and evaluation of an easily fabricated micromixer with three-dimensional periodic perturbation. *Chemical Engineering Journal, 171*(1), 291-300.

Liu, Z.-M., & Pang, Y. (2015). Effect of the size and pressure on the modified viscosity of water in microchannels. *Acta Mechanica Sinica, 31*(1), 45-52.

Liu, Z., Li, M., Pang, Y., Zhang, L., Ren, Y., & Wang, J. (2019). Flow characteristics inside droplets moving in a curved microchannel with rectangular section. *Physics of Fluids, 31*(2), 022004.

Liu, Z., Zhang, L., Pang, Y., Wang, X., & Li, M. (2017). Micro-PIV investigation of the internal flow transitions inside droplets traveling in a rectangular microchannel. *Microfluidics and Nanofluidics, 21*(12), 180.

Lobasov, A., Minakov, A., & Rudyak, V. Y. (2016). Viscosity effect on the flow patterns in T-type micromixers. *Fluid Dynamics, 51*(3), 381-388.

Ma, S., Sherwood, J. M., Huck, W. T., & Balabani, S. (2014). On the flow topology inside droplets moving in rectangular microchannels. *Lab on a Chip, 14*(18), 3611-3620.

Ma, S., Sherwood, J. M., Huck, W. T., & Balabani, S. (2015). The microenvironment of double emulsions in rectangular microchannels. *Lab on a Chip, 15*(10), 2327-2334.

Mahmud, F., & Tamrin, K. F. (2020). Method for determining mixing index in microfluidics by RGB color model. *Asia-Pacific Journal of Chemical Engineering*, e2407.

Meinhart, C., Wereley, S., & Gray, M. (2000). Volume illumination for two-dimensional particle image velocimetry. *Measurement Science and Technology, 11*(6), 809.

Meinhart, C. D., Wereley, S. T., & Santiago, J. G. (1999). PIV measurements of a microchannel flow. *Experiments in Fluids, 27*(5), 414-419.

Mondal, B., Pati, S., & Patowari, P. K. (2018). Numerical Analysis of Mixing Performance in Microchannel with Different Ratio of Outlet to Inlet Width. Paper presented at the *Proceedings of the 2nd International Conference on Advanced Technologies for Societal Applications*, Maharashtra, India.

Nagata, M. (2018). Usefulness of underwater endoscopic submucosal dissection in saline solution with a monopolar knife for colorectal tumors (with videos). *Gastrointestinal Endoscopy, 87*(5), 1345-1353.

Oishi, M., Kinoshita, H., Fujii, T., & Oshima, M. (2011). Simultaneous measurement of internal and surrounding flows of a moving droplet using multicolour confocal micro-particle image velocimetry (micro-PIV). *Measurement Science and Technology, 22*(10), 105401.

Omori, T., Imai, Y., Kikuchi, K., Ishikawa, T., & Yamaguchi, T. (2015). Hemodynamics in the microcirculation and in microfluidics. *Annals of Biomedical Engineering, 43*(1), 238-257.

Orsi, G., Roudgar, M., Brunazzi, E., Galletti, C., & Mauri, R. (2013). Water–ethanol mixing in T-shaped microdevices. *Chemical Engineering Science, 95*, 174-183.

Pang, L., Shen, S., Ma, C., Ma, T., Zhang, R., Tian, C., . . . Wang, J. (2015). Deformability and size-based cancer cell separation using an integrated microfluidic device. *Analyst, 140*(21), 7335-7346.

Pang, Y., Kim, H., Liu, Z., & Stone, H. A. (2014). A soft microchannel decreases polydispersity of droplet generation. *Lab on a Chip, 14*(20), 4029-4034.

Salim, A., Fourar, M., Pironon, J., & Sausse, J. (2008). Oil–water two-phase flow in microchannels: Flow patterns and pressure drop measurements. *The Canadian Journal of Chemical Engineering, 86*(6), 978-988.

Santiago, J. G., Wereley, S. T., Meinhart, C. D., Beebe, D., & Adrian, R. J. (1998). A particle image velocimetry system for microfluidics. *Experiments in Fluids, 25*(4), 316-319.

Shah, I., Kim, S. W., Kim, K., Doh, Y. H., & Choi, K. H. (2019a). Experimental and numerical analysis of Y-shaped split and recombination micro-mixer with different mixing units. *Chemical Engineering Journal, 358*, 691-706.

Shah, I., Su Jeon, H., Ali, M., Yang, D. H., & Choi, K.-H. (2019b). Optimal parametric mixing analysis of active and passive micromixers using Taguchi method. *Proceedings of the Institution of Mechanical Engineers, Part E: Journal of Process Mechanical Engineering, 233*(6), 1292-1303.

Shah, R., Shum, H., Rowat, A., Lee, D., Agresti, J., & Utada, A. (2008). CL Y., JW Kim, A. Fernandez-Nieves, CJ Martinez and DA Weitz. *Materials Today, 11*, 18-27.

Shen, F., Li, Y., Liu, Z., & Li, X. (2017). Study of flow behaviors of droplet merging and splitting in microchannels using Micro-PIV measurement. *Microfluidics and Nanofluidics, 21*(4), 66.

Shinohara, K., Sugii, Y., Aota, A., Hibara, A., Tokeshi, M., Kitamori, T., & Okamoto, K. (2004). High-speed micro-PIV measurements of transient flow in microfluidic devices. *Measurement Science and Technology, 15*(10), 1965.

Siddique, B. M., Ahmad, A., Ibrahim, M. H., Hena, S., & Rafatullah, M. (2010). Physico-chemical properties of blends of palm olein with other vegetable oils. *Grasas y Aceites, 61*(4), 423-429.

Solehati, N., Bae, J., & Sasmito, A. P. (2014). Numerical investigation of mixing performance in microchannel T-junction with wavy structure. *Computers & Fluids, 96*, 10-19.

Tamrin, K., Rahmatullah, B., & Samuri, S. (2015a). Aberration compensation of holographic particle images using digital holographic microscopy. *Journal of Modern Optics, 62*(9), 701-711.

Tamrin, K., Rahmatullah, B., & Samuri, S. (2015b). An experimental investigation of three-dimensional particle aggregation using digital holographic microscopy. *Optics and Lasers in Engineering, 68*, 93-103.

Teh, S.-Y., Lin, R., Hung, L.-H., & Lee, A. P. (2008). Droplet microfluidics. *Lab on a Chip, 8*(2), 198-220.

Thielicke, W. (2014). The flapping flight of birds. *Diss. University of Groningen.*

Thielicke, W., & Stamhuis, E. (2014). PIVlab–towards user-friendly, affordable and accurate digital particle image velocimetry in MATLAB. *Journal of Open Research Software, 2*(1).

Thurgood, P., Baratchi, S., Arash, A., Pirogova, E., Jex, A. R., & Khoshmanesh, K. (2019). Asynchronous generation of oil droplets using a microfluidic flow focusing system. *Scientific Reports, 9*(1), 1-11.

Turner, A., Yandrofski, K., Telikepalli, S., King, J., Heckert, A., Filliben, J., . . . Schiel, J. E. (2018). Development of orthogonal NISTmAb size heterogeneity control methods. *Analytical and Bioanalytical Chemistry, 410*(8), 2095-2110.

Viktorov, V., Mahmud, M. R., & Visconte, C. (2016). Numerical study of fluid mixing at different inlet flow-rate ratios in Tear-drop and Chain micromixers compared to a new HC passive micromixer. *Engineering Applications of Computational Fluid Mechanics, 10*(1), 182-192.

Vladisavljević, G. T., Al Nuumani, R., & Nabavi, S. A. (2017). Microfluidic production of multiple emulsions. *Micromachines, 8*(3), 75.

Vuckovac, M., Backholm, M., Timonen, J. V., & Ras, R. H. (2020). Viscosity-enhanced droplet motion in sealed superhydrophobic capillaries. *Science Advances, 6*(42), eaba5197.

Wang, B., Zhang, Y., Song, J., & Wang, Z. (2020). Investigation and Prediction on Regulation of Hydrophobicity of Polymethyl Methacrylate (PMMA) Surface by Femtosecond Laser Irradiation. *Coatings, 10*(4), 386.

Wang, H., Iovenitti, P., Harvey, E., & Masood, S. (2002). Optimizing layout of obstacles for enhanced mixing in microchannels. *Smart Materials and Structures, 11*(5), 662.

Wang, J., Wang, J., Feng, L., & Lin, T. (2015). Fluid mixing in droplet-based microfluidics with a serpentine microchannel. *RSC Advances, 5*(126), 104138-104144.

Wang, S., Huang, X., & Yang, C. (2011). Mixing enhancement for high viscous fluids in a microfluidic chamber. *Lab on a Chip, 11*(12), 2081-2087.

Wang, W., Zhao, S., Shao, T., Jin, Y., & Cheng, Y. (2012). Visualization of micro-scale mixing in miscible liquids using μ-LIF technique and drug nano-particle preparation in T-shaped micro-channels. *Chemical Engineering Journal, 192*, 252-261.

Wang, X., Liu, G., Wang, K., & Luo, G. (2015). Measurement of internal flow field during droplet formation process accompanied with mass transfer. *Microfluidics and Nanofluidics, 19*(3), 757-766.

Wu, B., von der Ecken, S., Swyer, I., Li, C., Jenne, A., Vincent, F., . . . Busse, F. (2019). Rapid Chemical Reaction Monitoring by Digital Microfluidics-NMR: Proof of Principle Towards an Automated Synthetic Discovery Platform. *Angewandte Chemie International Edition, 58*(43), 15372-15376.

Wu, Y.-A., Panigrahi, B., Lu, Y.-H., & Chen, C.-Y. (2017). An integrated artificial cilia based microfluidic device for micropumping and micromixing applications. *Micromachines, 8*(9), 260.

Xie, S., Yi, C., & Qiu, X. (2016). Salting-out effect of potassium pyrophosphate (K4P2O7) on the separation of biobutanol from an aqueous solution. *Journal of Chemical Technology and Biotechnology, 91*(6), 1860-1867.

Yadav, G., Maheshwari, S., & Agarwal, A. (2014). Contrast limited adaptive histogram equalization based enhancement for real time video system. Paper presented at the 2014 International Conference on *Advances in Computing, Communications and Informatics (ICACCI)*.

Yao, J., Lin, F., Kim, H. S., & Park, J. (2019). The effect of oil viscosity on droplet generation rate and droplet size in a T-junction microfluidic droplet generator. *Micromachines, 10*(12), 808.

Zhang, J.-w., Liu, S.-f., Cheng, C., Li, W.-f., Xu, X.-l., Liu, H.-f., & Wang, F.-c. (2019). Investigation of three-dimensional flow regime and mixing characteristic in T-jet reactor. *Chemical Engineering Journal, 358*, 1561-1573.

Zhu, P., Tang, X., & Wang, L. (2016). Droplet generation in co-flow microfluidic channels with vibration. *Microfluidics and Nanofluidics, 20*(3), 47.

Zhu, P., & Wang, L. (2017). Passive and active droplet generation with microfluidics: a review. *Lab on a Chip, 17*(1), 34-75.

Zhu, Q., Pan, Y., Jia, X., Li, J., Zhang, M., & Yin, L. (2019). Review on the stability mechanism and application of water-in-oil emulsions encapsulating various additives. *Comprehensive Reviews in Food Science and Food Safety, 18*(6), 1660-1675.

APPENDICES

Journal Publications

1. **Ringkai, H.**, Tamrin, K. F., Sheikh, N. A., & Barroy, P. (2021). Characterization of dissimilar liquids mixing in T-junction and offset T-junction microchannels. *Proceedings of the Institution of Mechanical Engineers, Part E: Journal of Process Mechanical Engineering, 235*(6), 1797-1806.
2. **Ringkai, H.**, Tamrin, K. F., Sheikh, N. A., & Mohamaddan, S. (2021). Evolution of Water-in-Oil Droplets in T-Junction Microchannel by Micro-PIV. *Applied Sciences*, *11*(11), 5289.